Plant resilience and extinctions through the Permian to Middle Triassic on the North China Block: A multilevel diversity analysis of macrofossil records

Conghui Xiong, Jiashu Wang, Pu Huang, Borja Cascales-Miñana, Christopher J Cleal, Michael J Benton, Jinzhuang Xue

Plant resilience and extinctions through the Permian to Middle Triassic on the North China Block: a multilevel diversity analysis of macrofossil records

Conghui Xiong[a], Jiashu Wang[b], Pu Huang[c], Borja Cascales-Miñana[d], Christopher J. Cleal[e], Michael J. Benton[e], Jinzhuang Xue[b,*]

[a] School of Earth Sciences & Key Laboratory of Mineral Resources in Western China (Gansu Province), Lanzhou University, Lanzhou 730000, PR China

[b] The Key Laboratory of Orogenic Belts and Crustal Evolution, School of Earth and Space Sciences, Peking University, Beijing 100871, PR China

[c] Nanjing Institute of Geology and Palaeontology, Nanjing 210008, P. R. China

[d] CNRS, University of Lille, UMR 8198-Evo-Eco-Paleo, F-59000 Lille, France

[e] School of Earth Sciences, University of Bristol, Bristol BS8 1RJ, United Kingdom

* Corresponding author. E-mail address: pkuxue@pku.edu.cn (J. Xue).

ABSTRACT

A key question about the end-Permian mass extinction (EPME) is why it has been so hard to determine its impact on land plants: some analyses show a very clear loss of diversity and yet others show little change. Perhaps the key issue is the scale at which the diversity data are analysed. Here we investigate plant diversity changes through the Permian to Middle Triassic in the North China Block (NCB) based on an updated dataset and diversity measured at different geographic-temporal scales. We define regional-scale diversity for the whole (palaeo)continent, including diverse depositional environments with plant fossils; landscape-scale diversity for a local area within the same depositional system, such as a fluvial or deltaic system; and bed-scale diversity for an individual bed formed in a relatively short time (e.g. less than 10,000 years). The floras from the Taiyuan, Shanxi, Lower Shihhotse, and Upper Shihhotse formations, and their lateral equivalents, seem to be relatively continuous and stable, dominated by wetland assemblages, with comparable diversities at bed, landscape and regional scales, and relatively stable extinction, origination, and turnover rates. The transition between the Upper Shihhotse and Sunjiagou formations (and lateral equivalents) saw the largest extinction of regional-scale generic and species diversity, with high extinction rates and low origination rates, but only slight changes in average bed-scale and landscape-scale diversities. After this, coal swamps disappeared, most widespread genera became extinct or shrank in distribution area, red beds became common, and surviving plants were walchian conifers, peltasperms and other advanced gymnosperms, indicating an overall drying trend in climate. A further extinction event happened at the transition between the Sunjiagou and Liujiagou formations (and lateral equivalents), with the highest species extinction and origination rates at regional scale. Almost all Permian plant species became extinct and were replaced by new taxa, while the bed-scale and landscape-scale diversities changed little. The Sunjiagou/Liujiagou transition event correlates with the marine EPME and the collapse of

Gigantopteris-dominated communities in southwestern China, and probably represents the terrestrial equivalent of the EPME in the NCB.

Keywords: Fossil record; Extinction; Vascular plants; Diversity; Permian; Triassic; North China

1. Introduction

The diversification of life through geological time showed different patterns on land and in the sea (e.g. Benton, 2001, 2010; Cascales-Miñana et al., 2010, 2018; Xiong and Wang, 2011; Cascales-Miñana and Cleal, 2013; Cascales-Miñana, 2016; Feng et al., 2020). Studies of the fossil record of marine faunas identify the famous "Big Five" mass extinctions and other evolutionary events in the sea (Sepkoski, 1979; Raup and Sepkoski, 1982; Bambach, 2006; Shen et al., 2011; Harper and Servais, 2018; Fan et al., 2020). Compared to the marine fossil record, the terrestrial counterpart is patchier and more incomplete, particularly for vascular plants, and thus needs more consideration of potential sampling and taphonomic biases (e.g. Niklas and Tiffney, 1994; Cleal et al., 2012; Cascales-Miñana et al., 2013; Xue et al., 2018). However, numerous studies have demonstrated that, with appropriate methodologies, true diversity signals can be extracted from the terrestrial fossil record, which indeed is the most important source of information for understanding the evolution of life on land (e.g. Knoll et al., 1979; Niklas and Tiffney, 1994; Cleal et al., 2012; Benton et al., 2013; Cascales-Miñana et al., 2013).

This paper stems from the ideas of Cleal et al. (2012, 2021), who used a hierarchy of diversity measures, according to different geographical scales, to describe the plant diversity changes in Carboniferous wetlands of western Europe and eastern North America. By following Whittaker et al. (2001) with some modifications, Cleal et al. (2012, 2021) suggested three levels of diversity suitable for studying the plant fossil record: local-scale diversity refers to species richness within

an area of ca. 0.1 ha, which is considered to correspond to the vegetation represented by macrofossils from a single locality; landscape-scale and regional-scale diversities refer to species richness within areas up to and more than 10^5 km^2 respectively. These suggested values for the area limit of each spatial scale provide a criterion for comparison, although they could be adjusted for different regions; other organisms such as terrestrial vertebrates may have different area limits in light of their different ecological strategies. It is well known that variations of local-, landscape- and regional-scale diversities are different and are driven by distinct factors (Geiger et al., 2009; Valdés et al., 2015). Measuring diversity at different scales is a practical way to get a better understanding of the nature of the fossil record and to reveal true biological signals. Thus, extrapolation of the methodology developed in Cleal et al. (2012, 2021) to study plant fossil records from other continents and other geological times should be promising. This paper represents such an effort and focuses on the Permian–Middle Triassic plant macrofossils from the North China Block (NCB).

The NCB has been an important source of various floras from the Carboniferous to Triassic (e.g. Gu and Zhi, 1974; Li et al., 1995; Cleal and Wang, 2002; Wang et al., 2002a, b, 2012, 2021). In the past decades, terrestrial strata and the contained plant fossils in the NCB have been extensively studied, yielding a good fossil record for analyses of long-term diversity dynamics at a regional scale. Some floras have been well documented, such as the Yuzhou flora comprising 111 genera and 307 species of plants (Yang, 2006; Yang and Wang, 2012), the assemblages from Weibei Coalfield with 66 genera and 209 species (Wang, 2010), and the Wuda tuff flora with *in situ* forests preserved as a vegetational Pompeii (Wang et al., 2012, 2021). Based on such a rich fossil record, however, there have been only limited quantitative studies of their palaeodiversities. Among these, Wang (1989) first studied fluctuations in standing diversity of plant macrofossil from the Permian of NCB; later, Shen et al. (1997) described the diversity evolution of plants from

the Permian of the North Qilian area, a part of the NCB; and more recently, Bond et al. (201) and Stevens et al. (2011), based mainly on Halle (1927)'s collection from Shanxi Province, recognized three extinction episodes among the Permian floras.

The accumulation of data in recent decades, with respect to the description of both many new floras and new chronostratigraphic data (e.g. Wang et al., 2012; Wu et al., 2021; Lu et al., 2021) means that analyses based on an updated database are required. In this article, we aim to analyse vegetation diversity changes at different spatial scales and provide an updated observation of major extinction events, based on a newly compiled database of plant macrofossils from the Permian to Middle Triassic of the NCB.

2. General remarks on stratigraphy

The NCB is bounded to the north by the east sector of the Central Asian Orogenic Belt and to the south by the Qilian-Qinling-Dabie Mountains of the Central Orogenic Belt of China, and further to the south is the South China Block (e.g. Huang et al., 2018, their Fig. 1). The NCB occupied a low-latitude position through the Permian to Middle Triassic in some palaeogeographic reconstructions (Fig. 1A; Huang et al., 2018), while in other schemes it drifted north of 30ºN during the Early and Middle Triassic (Scotese, 2001; Boucot et al., 2013). Through the Late Palaeozoic to Triassic, the NCB mainly supported terrestrial siliciclastic deposits bearing abundant plant fossils, but there were also some shallow marine deposits with animal fossils such as conodonts and fusulinids, facilitating stratigraphic dating and correlation (Jin et al., 2000).

According to Jin et al. (2000), the NCB can be divided into four subregions in terms of the Permian strata, including (Fig. 1B): the Jin-Ji-Lu Subregion (including southwestern part of the Inner Mongolia, northeastern Ningxia, Shanxi, northern Shaanxi, northern Henan, northern-central Shandong and southern Hebei provinces); the North Qilian Subregion (including areas of northern

Qilian Mountain, Longshou Mountain and western Helan Mountain); the Daqingshan Subregion (including southern-central Inner Mongolia, Beijing, northern Hebei, Liaoning and southern Jilin provinces); and the Huang-Huai Subregion (including southern-central Henan, southern Shaanxi, southern Shandong, northern Anhui, and northern Jiangsu provinces).

In the Jin-Ji-Lu Subregion, Permian strata are characterized by a well-known sequence, in ascending order comprising the Taiyuan, Shanxi, Lower Shihhotse, Upper Shihhotse, and Sunjiagou formations. The names of these lithological units are also used in other subregions, but some papers instead employ different lithological names in different subregions. A suggested correlation scheme for different units is provided here, as the basis for diversity statistics of plant genera and species (Fig. 2). A detailed discussion about the stratigraphy of the four subregions is provided in Appendix 1.

It should be noted that correlation of the Permian strata of the NCB to the standard international chronostratigraphic stages remains much debated, and different schemes have been suggested by different authors (e.g. Hilton and Cleal, 2007, their Fig. 4; Wang, 2010, his Fig. 10; Liu, 2018, his Fig. 1; Shen et al., 2019b, their Fig. 5; Wu et al., 2021, their Fig. 2; Lu et al., 2021, their Fig. 2). Traditionally, the correlation among different sections was based on data of plant macrofossil assemblages and/or palynology. For instance, Wang (2010) provided a review of the Late Palaeozoic plant macrofossil assemblages from the sequence through the Taiyuan to Sunjiagou formations; and Liu et al. (2015) proposed eight palynological biozones for the same formations. More recently, Wu et al. (2021) presented a new chronostratigraphic framework for the Permian succession of the NCB, based on high-precision U-Pb chemical abrasion-isotope dilution-thermal ionization mass spectrometry (CA-ID-TIMS) geochronology of tuffs. The order and correlation of formations remains the same (Fig. 2), but their matching to the international time

scale differs substantially through the bulk of the Permian, except the beginning (Asselian) and end (Changhsingian). For a more recent discussion of these discrepancies see Lu et al. (2021).

Over large areas of the NCB, Early and Middle Triassic strata are represented by the Liujiagou, Heshanggou and Ermaying formations. The Liujiagou Formation bears the *Pleuromeia jiaochengensis*-*Crematopteris circinalis* assemblage, distinct from plant macrofossils from the underlying Sunjiagou Formation (Wang and Wang, 1989). The Heshanggou Formation bears the *Pleuromeia sternbergii*-*Crematopteris* cf. *typica* assemblage, similar to the "Buntsandstein" flora of Europe, and the age of this formation was suggested to be Olenekian (Wang and Wang, 1990a; Li et al., 1995). The age of the underlying Liujiagou Formation was thus deduced to be Induan (Wang and Wang, 1989; Li et al., 1995). The age of the Ermaying Formation is suggested to be Anisian, based on the vertebrate *Sinokannemeyeria* association and CA-TIMS U-Pb zircon dating (Liu et al., 2018). In Zhifang, Tongchuan City of Shaanxi Province, the Zhifang Formation was identified as coeval withthe Ermaying Formation (Wang et al., 2019). The correlation of other lithological units to the Liujiagou, Heshanggou and Ermaying formations is provided in Appendix 1.

3. Data matrix of plant macrofossils, analytical methods and rationale

3.1. Compilation of plant macrofossil records

We collected from the literature all published plant macrofossil records at the species level, including those with open nomenclature such as sp. and cf., and information about their stratigraphy and localities. The fossil records were divided approximately into the Jin-Ji-Lu, North Qilian, Daqingshan, Huang-Huai subregions, as noted above. Within each subregion, the species names were listed according to different stratigraphic units, such as the Taiyuan, Shanxi, Lower Shihhotse formations, etc. Our data were updated until Dec. 30, 2019 and are shown in Appendix 2.

After this date, there have been a number of taxonomic descriptions of new taxa from different formations, but we consider that the addition of new data will have little effect on the overall taxonomic diversity trends obtained from the present dataset.

Based on the stratigraphic correlation discussed above (Fig. 2; Appendix 1), we divided the fossil records into eight stratigraphic units (thus, eight intervals) in ascending order: the middle-upper part of the Taiyuan Formation and its equivalents (TY interval); the Shanxi Formation and its equivalents (SX interval); the Lower Shihhotse Formation and its equivalents (LS interval); the Upper Shihhotse Formation and its equivalents (US interval); the Sunjiagou Formation and its equivalents (SJG interval); the Liujiagou Formation and its equivalents (LJG interval); the Heshanggou Formation and its equivalents (HSG interval); and the Zhifang and Ermaying formations and their equivalents (Z&E interval). Such a scheme is convenient for discussion and comparisons with other studies, since these stratigraphic units are commonly used, although their ages remain debated. Further studies will lead to some adjustments of the correlation scheme, thus demanding corresponding adjustment of the diversity patterns revealed here; however, our data are presented clearly enough for necessary revisions for the time scale.

A key problem with palaeobotanical diversity studies is that a single biological entity might be represented by several fossil-taxa for each of the different plant parts, and so will be represented in the literature by multiple taxonomic names (Cleal et al., 2021; Cleal and Thomas, in press). For example, the Carboniferous lycopsid tree *Lepidodendron* is famously given multiple names: *Stigmaria* (roots), *Lepidodendron* (stems), *Lepidostrobophyllum* (dispersed sporophylls), *Cyperites* (stem leaves), and *Lepidostrobus* (microsporangiate cones), among others (e.g. Cleal et al., 2021, their fig. 4). Not recognising this would lead to artificial inflation of taxa. One solution is to use the fossil-taxa for foliage or related structures for each plant group, and to exclude those based on other organs; this approach was used by Cleal et al. (2012). Here we argue that the

preserved plant parts likely represent only a subset of the "actual" number of the plants that once lived, and that including all different plant parts in the diversity estimation provides a different view from those based only on, for instance, foliage taxa. On the other hand, counting only foliage taxa may cause possible underestimation of the "real" plant diversity, because some plants might not be represented by their leaves or related structures in the fossil record. For instance, the vegetative stem leaves of arborescent lycopsids (e.g. the fossil-genus *Cyperites*) have been rarely recorded in the fossil record of the NCB. In our dataset, we make a test for the above inflation or underestimation effects by distinguishing the foliage genera (and their species) from non-foliage ones, and for the eight intervals, estimate the percentages of non-foliage taxa in the total diversity (Table 4). The percentages of non-foliage genera in six of the eight intervals range from 20% to 25%, while the percentages for the TY and Z&E intervals are 38% and 9%, respectively, and, for the analyses that include or exclude non-foliage taxa, the regional-scale diversities show consistent trends except for the TY and Z&E intervals (Fig. 11A). For this reason, we do not exclude non-foliage taxa from our analyses of bed-scale, landscape-scale, and regional-scale diversities.

3.2. Bed-scale diversity

Based on the methodology of Cleal et al. (2012), with some modifications, Figure 3 presents our working model and rationale. For each interval, we selected some well-studied, representative sections, and collected from the original literature, bed by bed, information on bed thickness, lithology, and plant species in each section (Table 1; Appendix 3). The bed thickness in the original descriptions is variable; some beds were described as being less than 1 m in thickness, and others were over ten metres or more. Thus, for mudstones and siltstones, beds less than or about 10 m thick were selected, while for sandstones, there were no thickness limits. For each bed, the species

richness, S_{bed} for simplicity was counted and analyzed (Tables 1 and 3) as this is widely recognised to be a robust measure of the ecological structure of a flora (Magurran, 2004; Pardoe et al., 2021).

There are two limitations in our dataset. First, the bed thickness of fine sediments in the literature varies from several centimetres to ca. 10 m. However, there is no significant correlation between bed thickness and number of species contained in these beds (Fig. 4A), indicating that bed thickness is not a controlling factor of plant diversity. Also, it cannot simply be generalized that thicker beds indicate longer depositional times because of different depositional rates in different settings. Shen et al. (2015) demonstrated that the aggradation rates of floodplains and delta-plains can reach 10–40 mm per year, and thus the aggradation of a 10-m-thick mudstone profile may take only 250 to 1,000 years (see also Gastaldo, 1985; Gastaldo et al., 1995). For the first four intervals (TY, SX, LS and US), the studied floras are mostly from fine sediments that are associated with or above coal seams, and as claimed by Cleal et al. (2012), the depositional processes for such floras, mostly being overbank flooding, would have been rapid. It is generally considered that the sandstone beds that are usually thick would have been formed in a high-energy environment with high depositional rates. Thus, the plants within a single bed represent either an instantaneous (T_0) snapshot of the local vegetation, or a time-averaged assemblage over a relatively short time (e.g. less than 1,000 years, or more broadly, less than 10,000 years). Second, based on the original descriptions, it is difficult to determine whether the plants within these beds are autochthonous, parautochthonous or allochthonous (Gastaldo et al., 1995; Pardoe et al., 2021). It is more likely that the plants within conglomerate or sandstone beds, mainly from the SJG and LJG intervals, are allochthonous. For the mudstone / siltstone beds, autochthonous or parautochthonous burial might be more common. We argue that, however, the allochthonous assemblages also contain vegetation information at a local scale, because: (1) labile foliages, with high rate of decomposition (Gastaldo and Demko, 2011), are very abundant in our dataset; and (2) long-distance postmortem transported

fragments seem to be rare, even if present. Nevertheless, on account of the above limitations, we consider that the bed-scale diversity in our study is not strictly equal to, but instead an approximation of, the local-scale diversity of Cleal et al. (2012). By their definition, the local-scale diversity means "species diversity within an area of c. 0.1 ha, which effectively corresponds to the vegetation represented in the macroflora from a single fossil locality." Our bed-scale diversity is also an approximation of the within-habitat species diversity of Knoll et al. (1979), a measure that is the total number of species in a given flora, and of the alpha-diversity, which represents the species number in an individual habitat (Hofmann et al., 2017).

3.3. Landscape-scale diversity

For each interval, nearby localities with comparable lithological sequences, which have been documented to have accumulated in the same depositional system such as a fluvial, coastal, or deltaic system, were grouped together. Localities of the same group were plotted on the map, and then the minimum area that covers these localities were delimited by a convex hull, using the software Arcmap 10.2. We call this convex hull a **geographic patch** (or simply, **patch**), whose area can be measured. By doing this, we divided the fossil records of each interval into different patches, ranging in area from 10^4 to 10^5 km^2, to represent diversity at the landscape scale (Table 2; Fig. 5). The genus and species numbers within each patch (G_{pat} and S_{pat}) were counted, and the relationship between G_{pat} (or S_{pat}) and the patch areas was investigated by correlation analyses. For each interval, the accumulation curves of G_{pat} and S_{pat}, along with the stepwise addition of patches to the pool, were also drawn.

Species distribution maps of the patches for each interval are shown in Figure 5. These kinds of maps are intuitive and useful for demonstrating the geographical patterns of organisms at the regional or global scale (Di Marco et al., 2016; Dyer et al., 2017). However, plots of species

diversity of fossil organisms often suffer from incomplete sampling, so our approach is to show differences between the patches within each interval, and changes in species diversity through the time intervals. The patches are colour coded according to levels of S_{pat} in the species distribution maps, which were calculated in the software Arcmap 10.2.

Network analysis (NA) is used to study and visualize the biogeographic structure of the floras and the connections and provincialism of organisms through geological time (Kiel, 2017; Huang et al., 2018). For each interval, a matrix was compiled for absence/presence of plant genera across the geographic patches for analysis by NA. The network diagrams generated by NA show how a patch is connected to others via shared genera. As shown in Figure 10, the larger nodes represent different patches, the smaller nodes represent plant genera, and the patches are connected to each other by lines linking shared genera; genera that occur in one only patch are plotted outside the corresponding patch, with a single line. Three attributes of the network were calculated for each interval, namely the average degree (AD), graph density (GD), and modularity (MD). For a given network, the AD is the number of lines divided by the number of nodes; the GD is the ratio of the number of lines to the number of all potential lines; and the MD is an index of network clustering, where a higher MD value indicates the nodes are more tightly connected or clustered (see Huang et al., 2018 for detailed explanation). The analyses were conducted in the Gephi software package (www.Gephi.org), based on methods introduced by Huang et al. (2018) and Wang and Huang (2020). The following settings were used: Force Atlas; Inertia 0.1; Repulsion strength 40000.0; Attraction strength 10.0; Maximum displacement 10.0; Auto stabilize function true; Autostab Strength 80.0; Autostab sensibility 0.2; Gravity 30.0; and Speed 1.0.

3.4. Regional-scale diversity

Diversity across the whole NCB, ca. 2.7 $\times 10^6$ km^2 in area, can be considered to represent the regional-scale diversity. Based on the data from all localities of each of the eight intervals, the genus and species richnesses, G_{tot} and S_{tot}, were calculated for each interval. Because of the great debate concerning the age of the Permian sequence of the NCB (Fig. 2), we cannot define the durations of the eight intervals, and thus we did not calculate the diversity per million years.

Extinction rates (*ER*), origination rates (*OR*), and turnover rates (*TR*) are important parameters that are commonly used in diversity analysis (see e.g. Xiong and Wang, 2011; Cascales-Miñana et al., 2013, and references therein). For each interval, we calculated these rates according to the formulas:

$$ER = N_e / N_{tot} \qquad (1)$$

$$OR = N_o / N_{tot} \qquad (2)$$

$$TR = (N_e + N_o - SL) / N_{tot} \qquad (3),$$

where, N_e means the number of genera/species that became extinct in the studied interval, N_o, the number of genera/species that newly appeared in the studied interval, and *SL*, the number of genera/species that occurred only in the studied interval.

Then, we adopted the methodology of polycohort analysis used in Cleal et al. (2012) and plotted the survivorship curves for the genera and species. This method takes all the taxa that exist in an interval and plots their percentage survivorship through successive intervals.

3.5. Heterogeneity among sections

In ecology, heterogeneity is defined to evaluate differences in composition in different areas, and so can indicate isolation effects caused by distance or geographical barriers and changes in species composition along an environmental gradient (Kolasa and Rollo, 1991). Here, for each interval, we first selected some representative sections, calculated pairwise Heterogeneity Index

(*HI*) values at the generic level between pairs of sections, and then obtained the average and standard deviation of the pairwise *HI* values. For sections a and b, the pairwise *HI* was calculated as:

$$HI = G_n/G_{ab} \qquad (4)$$

where, G_n is the number of genera not shared by sections a and b, and G_{ab} the total number of genera in sections a and b.

The data processing mentioned above was performed using the software Excel and PAleontological STatistics (PAST) (Hammer et al., 2001).

4. Results

4.1. Diversity pattern in the TY, SX, LS and US intervals

4.1.1. Bed-scale diversity

The bed-scale species richness (S_{bed}) shows a large range (Fig. 4): 2–40 species for the TY interval; 1–55 species for the SX interval; 1–29 species for the LS interval; and 1–21 species for the US interval. However, most beds contain < 10 species. The median value of S_{bed} rises from the TY interval to the SX and LS intervals, and then declines slightly in the US interval (Fig. 6), while, statistically, the differences of the medians among the four intervals is not significant (Kruskal-Wallis test, $X^2 = 3.386$, $p = 0.3343$). The highest value occurs in the Shanxi Formation of the Longwanggou section, Inner Mongolia, where a 6.3-m-thick mudstone bed contains ca. 55 species (Table 1), including species of *Sphenophyllum*, *Calamites*, *Annularia*, *Lobatannularia*, *Pecopteris*, and others (Appendix 3.2; He et al., 1990).

4.1.2. Landscape-scale diversity

Seven geographic patches were created for the TY interval, shown as TY1 to TY7 in Figure 5A. A locality at Zibo, isolated from other localities, may form another patch, but the area of this patch is much smaller than the other patches. The seven patches range from 0.92–8.80 × 10^4 km^2 in area (Table 2). The total area of the seven patches reaches 4.05 × 10^5 km^2, supporting 75 genera and 221 species. The genus and species richnesses (G_{pat} and S_{pat}) in TY2 are highest, with 44 genera and 98 species.

Seven patches, SX1 to SX7, were created for the SX interval (Fig. 5B). The localities around Dongheishan are isolated, forming a limited patch area. The seven patches range from 2.08–13.06 × 10^4 km^2 in area (Table 2). The total area of these patches is 4.09 × 10^5 km^2, supporting a total diversity of 125 genera and 490 species. Patch SX1 contains the highest diversity, with 83 genera and 271 species.

There are also seven patches in the LS interval, termed LS1–LS7 (Fig. 5C). The localities around Dongheishan form a much smaller one. The seven patches range from 3.48–12.55 × 10^4 km^2 in area (Table 2). The total area is 5.50 × 10^5 km^2, and the total diversity increases to 143 genera and 635 species. The highest genus and species diversity occur in LS1, with 100 genera and 400 species.

Eight patches, from US1 to US8, were created for the US interval (Fig. 5D), ranging from 3.28–16.85 × 10^4 km^2 in area (Table 2). The total area reaches its largest value (7.07 × 10^5 km^2) in the Permian, with a total diversity of 152 genera and 597 species. The patch US1 contains the highest diversity, with 103 genera and 316 species.

To sum up, the median values of G_{pat} and S_{pat} increase from the TY interval to the SX interval, slightly decreases in the LS interval, and then rebounds in the US interval (Fig. 7A, B). However, statistically, the medians of G_{pat} and S_{pat} for the four intervals are not significantly different (Kruskal-Wallis test: $X^2 = 5.955$, $p = 0.1134$ for G_{pat}; $X^2 = 6.869$, $p = 0.076$ for S_{pat}).

Generally, the larger the patch area, the more genera and species are found (Fig. 8A–D). Nevertheless, for each of the four intervals, the correlation between patch area and plant diversity (G_{pat} and S_{pat}) is not significant (Fig. 8A–D). As total area increases by the stepwise accumulation of patches, the curves for increasing G_{pat} and S_{pat} appear to approach equilibrium (Fig. 9). When compared within the same cumulative area of about 4.0×10^5 km^2, the corresponding diversity of the TY interval is considerably lower than for the other three intervals.

Species distribution maps (Fig. 5A–D) show that the patches of the TY interval generally support a lower diversity than in the other three intervals. The southern part of the NCB shows a patch with more than 200 species in each of the SX, LS and US intervals (patches SX1, LS1 and US1), indicating stable development of high-diversity floras over the region. Diversity of the middle part of the NCB is highest in the LS interval, with one patch (LS2) supporting more than 200 species. In the northern part of the NCB, patch SX2 is the only one with more than 200 species.

Network analysis shows overall consistency for the networks of the four intervals (Fig. 10A–D), and the values of the average degree and modularity are also consistent (Table 7). However, the graph density of the network for the TY interval is higher than for the other three intervals, because of lower generic diversity in the patches (i.e. Fig. 9A). For these four intervals, connections of patches by shared plant genera is dense, with very complex patterns, while some patches show high percentages of endemics (Fig. 10A-D).

4.1.3. Regional-scale diversity dynamics

Regional-scale diversity, across the whole of the NCB (Table 4; Fig. 11A), shows progressive increase of generic richness from the TY interval (76 genera) to the US interval (highest value of 152 genera). Species richness increases greatly through the TY interval to the LS interval, reaching peak of 643 species, then decreases slightly during the US interval.

The extinction rates of genera and species progressively increase from the TY/SX transition, SX/LS transition, to the LS/US transition; generic extinction rate ranges from 0.28–0.43, and species extinction rate ranges from 0.48–0.62 (Table 5; Fig. 12A, B). Showing an opposite trend to the extinction rates, species origination rates (Table 5; Fig. 12A, B) decrease progressively from the TY/SX transition, SX/LS transition, to the LS/US transition, with values ranging from 0.77–0.59. The genus origination rate is higher at the TY/SX transition, and lower at the SX/LS and LS/US transitions. Turnover rates show a decline from the TY/SX transition to the SX/LS transition, and then rebound a little at the LS/US transition.

Polycohort analyses (Table 6; Fig. 13A, B) show that the plant genera and species first occurring in the TY interval (the TY genera or species for simplicity) gradually disappear in the subsequent three intervals. The survival percentage of TY genera is 72% in the SX interval, 67% in the LS interval, and 57% in the US interval, and the survival percentage of TY species is 52% in the SX interval, 45% in the LS interval and 30% in the US interval. Thus, the TY/SX transition saw the greatest magnitude of loss of TY genera and species. SX plants show survival of 67% genera and 49% species in the LS interval and 51% genera and 32% species in the US interval; again, the greatest magnitude of diversity loss occurs at the SX/LS transition. LS plants show survival of 57% genera and 38% species in the US interval.

The average values of the heterogeneity index are comparable through the four intervals (Table 4; Fig. 11B). This means that, for different intervals, differences among different sections are comparable.

4.2. Diversity patterns across the US/SJG transition

Available data for the estimation of bed-scale diversity (S_{bed}) of the SJG interval are limited, from limited descriptions of fossil plants and information on detailed bed thicknesses. Only five

beds of this interval were considered, and S_{bed} ranges from 1–9 (average, 4). Three beds were recorded as fine-grained sandstone, with thinly bedded mudstone, and two others are mudstone or siltstone. Apparently, the average bed-scale diversity declines considerably from the US interval to the SJG interval (Tables 1 and 3; Figure 5). However, the difference of the median S_{bed} between these two intervals is not significant (Mann-Whitney test, z = -1.533, p = 0.1254).

Species distribution maps across the NCB also show a rapid change of species diversity before and after the SJG interval and subsequently. The TY-to-US intervals show more patches, larger sum area of the patches, and higher diversity; and the SJG-to-Z&E intervals show fewer patches, smaller sum area of the patches, and lower diversity. The number of plant-bearing localities is much lower in the SJG interval, and only four patches, SJG1–SJG4, were created here (Fig. 5E). The four patches range from 2.26×10^4 km^2 (SJG3) to 4.51×10^4 km^2 (SJG1) in area, with a total area of 1.34×10^5 km^2. The total diversity, 56 genera and 97 species, decreases greatly compared with the TY-to-US intervals. Patch SJG1 contains the largest diversity, with 21 genera and 34 species. The US/SJG transition saw the decline of the average G_{pat} from 45 to 19 and the decline of the average S_{pat} from 116 to 27 (Table 3; Fig. 7). The difference in median S_{pat} between the US and SJG intervals is significant at an alpha level of 0.1 (Mann-Whitney test: z = -1.953, p = 0.0508), while the difference in median G_{pat} betweenf the US and SJG intervals is not significant (Mann-Whitney test: z = -1.613, p = 0.1066).

There were great changes in the three attributes of the patch-genus networks across the US/SJG transition (Table 7), indicating substantial changes in the distribution patterns of plants (Fig. 10). Across this transition, the decrease in average degree and increase in graph density might reflect a rapid decline of total diversity in the network, while the increase in modularity value indicates that the patches are more tightly connected in the SJG interval. For instance, the patches

SJG3 and SJG4 show no or few endemics. The network pattern of the SJG interval is followed in the LJG and HSG intervals.

The regional-scale diversity reduces greatly from 152 genera and 597 species in the US interval to 58 genera and 100 species in the SJG interval, and afterwards, total diversity did not recover to a level comparable to that in the TY-to-US intervals. The heterogeneity indices among sections are consistent between the US and SJG intervals (Table 4; Fig. 11B).

Across the US/SJG transition, the genus extinction and turnover rates are 0.76 and 0.79 respectively, and the species extinction and turnover rates reach 0.94 and 0.95 respectively, indicating that substantial changes occurred in floristic composition. Across this transition, the genus origination rate is 0.36, the smallest value through the eight studied intervals, and the species origination rate is 0.65, among the lower values of the studied intervals, indicating limited speciation.

Polycohort analysis shows most plant genera and species disappeared at the US/SJG transition (Fig. 13). In the SJG interval, the surviving percentage of plant genera that first occur in the TY-to-US intervals is less than 30%, and the surviving percentage of the TY-to-US plant species, less than 6%. Thus, the extinction is serious at both generic and species levels, but more severe for species.

4.3. Diversity patterns across the SJG/LJG transition

In the LJG interval, we have data from only three beds to estimate bed-scale diversity (S_{bed}), showing one, six, and 11 species in the beds, and the diversity level is seemingly comparable with that of the SJG interval (Table 1; Fig. 5).

Compared to the SJG interval, the number of fossil localities decreases in the LJG interval, and we could create only two patches, LJG1 (5.52×10^4 km^2) and LJG2 (8.68×10^4 km^2) (Fig. 5F). The

localities near Yangshugou are limited in area. There are 20 genera and 34 species in the total 1.42 × 10^5 km^2 area. The G_{pat} and S_{pat} show a slight decline from the SJG to the LJG interval (Table 3; Fig. 7A, B).

Regional-scale diversity declines from 58 genera and 100 species in the SJG interval to 32 genera and 52 species in the LJG interval (Table 3; Fig. 11A). Two sections in the LJG interval are available for estimation of the heterogeneity index, with a value of 0.75, comparable to the average level of the SJG interval (Table 6; Fig. 11B). The SJG/LJG transition saw the highest levels of extinction, origination, and turnover rates of plant genera (0.88) and species (0.97) among all studied intervals (Fig. 12). These high turnover values show that the floras of the LJG interval are almost completely new compared to those of the SJG interval.

Polycohort analysis shows that almost all plant species occurring in the TY-to-US intervals became extinct in the LJG interval (the surviving percentage is ca. 2% or less; Table 6; Fig. 13). Only a very small proportion of the SJG floras continued in the LJG interval, and the surviving percentage is 17% for genera and 5% for species.

4.4. Diversity pattern in the Early to Middle Triassic

The records of bed-scale diversity in the HSG and Z&E intervals are limited. One bed in the HSG interval shows six species in a bed of 2-m-thick sandstone, and three beds in the Z&E interval show four, eight, and 20 species, respectively. Although the available data are limited, it is likely that the diversity level within a single bed is comparable with that of the preceding intervals.

Three patches HSG1, HSG2 and HSG3 were created in the HSG interval (Fig. 5G), of which HSG1 has the highest genus and species diversity, with 49 genera and 85 species in a 6.98 × 10^4 km^2 area (Table 2). The total diversity of the three patches is 53 genera and 99 species.

Two patches, Z&E1 (7.85×10^4 km^2) and Z&E2 (6.35×10^4 km^2), were created for the Z&E interval (Fig. 5H). Two localities Linjiawaizi and Qiandianzi form a much smaller patch. The Z&E1 patch has 40 genera and 64 species, and the Z&E2 patch 17 genera and 23 species (Table 2). There is a total of 46 genera and 75 species in the sum of the two patches (1.42×10^5 km^2 in total area). The median values of G_{pat} and S_{pat} remain low in the HSG interval but more than double in the Z&E interval (Table 3; Fig. 7A, B).

After the LJG interval, regional-scale diversity rebounds a little in the HSG and Z&E intervals but is still far lower than that in the LS and US intervals. The extinction rate of genera and species declines greatly at the LJG/HSG transition, but origination and turnover rates are higher at the LJG/HSG transition and the HSG/Z&E transition (Table 5; Fig. 12A, B).

Polycohort analysis shows that the genera arising in the LJG interval survived 53% to 59% in the HSG and Z&E intervals, and that the genera first occurring in the HSG interval survived 48% in the Z&E interval (Table 6; Fig. 13A, B). This indicates the floristic components across the interval boundaries of the Triassic are more similar, compared to the great turnover across the US/SJG and SJG/LJG transitions.

5. Discussion

5.1. Comparison with previous results

Wang (1989) was first to study diversity fluctuations of plant macrofossils at regional scale through the Permian to earliest Triassic of the vast area of the NCB (including Inner Mongolia, Liaoning, Hebei, Ningxia, Gansu, Shanxi, Shaanxi, and Henan). He recognized two major events: the first, at the US/SJG transition, which represents the replacement of Palaeophytic by Mesophytic floras as defined by Cleal and Cascales-Miñana (2014, 2021); the second, at the SJG/LJG transition, representing the terminal Permian mass extinction (Fig. 14). We confirm these

two events, now based on a much-enlarged dataset, with better dating, and from much wider coverage across the NCB.

Shen et al. (1997) noted a floral crisis at the base of the Yaogou Formation (corresponding to the base of the US interval here), with the extinction of more than half the plant species, based on their study of plant macrofossils from the Permian of the North Qilian area, the western part of the NCB (Fig. 14). However, we do not find this event, as our species distribution maps show an increase in both diversity and patch area in the western part of the NCB during the US interval (Fig. 5C, D, from patch LS4 to patch US3). Stevens et al. (2011) recognized three extinction episodes in Permian floras from North China, based on the collections of Halle (1927) from six localities in central Shanxi Province: in the Lower Shihhotse Formation with a loss of 45% of plant species, in the middle Upper Shihhotse Formation with a loss of 56% of species, and in the upper Upper Shihhotse Formation with a devastating loss of species. We suggest these are local-scale events, as Stevens et al. (2011) only sampled from within our patches TY3, SX3, LS2 and US2 (Fig. 5A–D), and their bed-by-bed comparisons through the Lower Shihhotse and Upper Shihhotse formations differ from ours in temporal resolution (Fig. 14). Our species distribution maps show a major loss of diversity in patch US2, probably corresponding to the last event of Stevens et al. (2011).

Our study indicates that diversity patterns differ in different subregions, as shown in our species distribution maps (Fig. 5). Patches containing more than 200 species (i.e. $S_{pat} > 200$) in our species distribution maps (Fig. 5, dark green areas) are located in northern and southern parts of the NCB during the SX interval, in central and southern parts during the LS interval, and only in the southern part during the US interval. Thus, from the SX to the US interval, there was a southward drift of highest diversity patches, and the destruction of floras across the NCB was not synchronous, occurring earlier in the north and later in the south. This trend correlates with the shift of the deposition centre of coal seams in the NCB (Liu, 1990, his figs. 5, 7, 8), in that thick coal

seams occur across large areas of the NCB in the TY and SX intervals but are limited to the southern part of the NCB in the LS and US intervals.

5.2. Stability and variability of the floras through the TY, SX, LS and US intervals

The floras of the TY, SX, LS and US intervals (TY-to-US, for simplicity) in the NCB are mainly preserved in coal-forming environments (e.g. Pfefferkorn and Wang, 2007; Wang, 2010; Wang and Pfefferkorn, 2013), matching the composition and ecology of Pennsylvanian floras from Euramerica (e.g. Hilton and Cleal, 2007; DiMichele et al., 2001; DiMichele, 2014; Thomas and Cleal, 2017). In Pennsylvanian Euramerica, both wetland vegetation and seasonally dry vegetation occurred, and they each dominated at different times under different climatic regimes (DiMichele, 2014). Our dataset did not differentiate between these two types of vegetation, since only a few original descriptions contained sedimentological and/or ecological data (e.g. Wang et al., 2012), while most records lacked such information. Pfefferkorn and Wang (2007) described four floras from a 4.32-m-thick section of the "Shanxi Formation" (corrected to Taiyuan Formation in later studies; see Wang et al., 2012), three of which are autochthonous and represent peat-forming communities, and one is parautochthonous and represents plants growing around a water body on a clastic substrate. These suggest spatial heterogeneity of landscapes and vegetations even in a single fossil site. Such distinctive plant assemblages also occurred earlier in Pennsylvanian-age lowlands including levee and floodplain vegetation (DiMichele and Nelson, 1989).

The bed-scale diversity of the TY-to-US intervals of the NCB is comparable to the local-scale diversity of the eastern part of the South Wales Coalfield, where species richness at the local scale is ca. 14 on average, with a range from 9–39 (Cleal et al., 2012, their Table 3). This compares well with our bed-scale species richness values of 8–13, although we did find some beds with over 50 species, suggesting great heterogeneity in the NCB Permian-Triassic floras. Our floras also exceed

some of the values suggested by Cleal et al. (2012) for landscape-scale species richness, ranging from 40–100 in an area of ca. 10^{-3} to 10^{5} km^2, based on the Pennsylvanian floras of Euramerica. The patches we delimited for the TY-to-US intervals in the NCB are comparable in area to the Pennines (6.70×10^4 km^2) and Ruhr (1.20×10^4 km^2) basins investigated by Cleal et al. (2012). The S_{pat} in the TY interval is estimated to be 48 on average, well within the range suggested by Cleal et al., but the mean S_{pat} for patches of the SX, LS and US intervals are much higher, at 126, 128, and 116, respectively. Several patches of the NCB contain more than 200 species, much higher than observed in the Pennines, Ruhr and South Wales basins of Euramerica; the reason for this may be due to the practices of splitting by taxonomists (e.g. Yang, 2006), and also, the European data were standardized by including only taxa for one plant part per plant group, while the Chinese data were not processed in the same way.

At the regional scale across the NCB, the polycohort analysis shows higher survival rates, with more than half of genera surviving, at the TY/SX, SX/LS, and LS/US transitions. The rates of extinction, origination and turnover are more-or-less stable, with relatively lower extinction rates and higher origination rates. In Weibei Coal Field, six species (*Lepidodendron oculus-felis*, *Stigmaria ficoides*, *Sphenophyllum oblongifolium*, *Calamites cistii*, *C. suckowii* and *Cordaites principalis*) were present throughout the TY-to-US intervals, and floras in the SX interval show great similarities to floras in later intervals, and ca. 41% of species in the TY-to-LS intervals persisted in the US interval (Wang, 2010). The Yuzhou floras from the southern part of the NCB show that ca. 75% of species are shared with the Zhutun and Shenhou formations; 67% of the Zhutun Formation species persisted into the Xiaofengkou Formation, and 57% of Xiaofengkou Formation species persisted into the Middle to Upper Yungaishan Formation (Yang, 2006). Li et al. (1995) suggested that floras in the LS and US intervals show high similarities, although they succeed each other in age. The dominant groups indicate gradual evolution, e.g. *Neuropteris*

ovata-Lepidodendron posthumii Assemblage in the upper TY interval, *Emplectopteris triangularis-Taeniopteris mucronata-Lobatannularia sinensis* Assemblage in the SX interval, *Emplectopteris triangularis-Tingia carbonica-Cathaysiopteris whitei* Assemblage in the LS interval, and *Gigantonoclea lagrelii-Lobatannularia ensifolia-Fascipteris hallei* Assemblage in the US interval (Li et al., 1995; Yang, 2006; Wang, 2010). These assemblages, with their comparable diversity, higher survival rates, and relatively stable extinction, origination and turnover rates, indicate that floras through the TY-to-US intervals were relatively continuous and stable.

The dominant plant assemblages in the NCB are distinct from coeval floras in Euramerica by many endemic elements, e.g. *Lobatannularia*, *Tingia*, *Cathaysiopteris*, *Cathaysiodendron*, *Emplectopteris*, *Emplectopteridium*, and *Gigantonoclea* (Li et al., 1995), and particularly, at the species level (Wang et al., 2012). The TY-to-US floras in the NCB comprise diverse lycopsids, ferns, sphenopsids, pteridosperms, and woody cordaitaleans, the floras of peat-forming landscapes of a wetland biome with humid to moist subhumid climate in the Late Palaeozoic, as also demonstrated in Euramerica Late Carboniferous floras (e.g. Galtier, 1997; Galtier and Daviero, 1999; Thomas, 2007; Thomas and Seyfullah, 2015; Bashforth et al., 2014, their Table 1). The relatively stable tropical coal-bearing floras in Euramerica persisted through much of the Pennsylvanian, lasting for about 10–30 Ma in different regions, and disappeared in parallel with the drying trend in the earliest Permian (Calder and Gibling, 1994; DiMichele et al., 2001; Cleal et al., 2012, 2018). The development of abundant coal-bearing floras coincided with the significant global climatic cooling of the Late Palaeozoic Ice Age, which reached its glacial maxima in the Pennsylvanian (late Bashkirian–Moscovian) and Cisuralian (Sakmarian) separated by a major interglacial during the Kasimovian, and then deglaciated after the Sakmarian (Gastaldo et al., 1996; Isbell et al., 2003). The coal-bearing floras in the NCB, located at a similar latitude to North

America in the Late Palaeozoic (Huang et al., 2018), flourished later than those in Euramerica, but probably lasted over a similar age range. This implies that the duration of the TY-to-US interval might be much shorter than previously thought. This could suggest that the time scale newly calibrated by Wu et al. (2021) is highly plausible, suggesting that the TY-to-US interval corresponds to the Asselian to Kungurian, the Cisuralian Epoch, at least in some parts of the NCB (Fig. 2).

5.3. Interpretation of the US/SJG transition event

As discussed above, the TY-to-US floras are overall stable and successive, with comparably high diversities. However, there is a major decline in regional-scale plant diversity from the US interval to the SJG interval, and the reduction in bed-scale and landscape-scale diversities is also likely, yet statistically not significant. Patch US1 in the south of the NCB shows more than 300 species, but this patch does not continue into the SJG interval when patch SJG3 is limited in area and has only 15 species. Patch US2 shows 183 species but shrank in area to patch SJG2 with only 50 species. The Sunjiagou Formation of the Wenquan Section, Henan Province is more than 800 m thick and has 92 beds dominated by sandstone and red mudstone, but identifiable plant fossils have been found in two only beds (Wang, 1997). The regional-scale diversity shows higher extinction rates, lower origination rates, and much lower plant survival percentages, indicating a severe plant extinction at this transition. Most widespread genera became extinct or shrank in their geographic distribution.

If the age determination provided by Wu et al. (2021) is correct, the suggested stratigraphic truncation, or unconformity, between the Upper Shihhotse and Sunjiagou Formations indicates an uplift of the NCB after the end of Cisuralian and before the re-start of sedimentation ca. 20 myr later. Thus, it is not surprising that there was a great disruption of floral development across the

US/SJG interval transition. Liu (1990) showed that depositional environments changed substantially from the TY-to-US to SJG intervals. Peat swamps fed by both rainwater and groundwater were widely distributed in the TY and SX intervals, forming thick coals across large areas of the NCB (Liu, 1990). In the LS and US intervals, coals with a thickness of more than 20 m became restricted to the southern part of the NCB, but coal-forming plant assemblages persisted in other areas. Based on the litho-geographical maps of Liu (1990), areas with >5-m-thick coal seams extend over ca. 1.20×10^6 km^2 in each of the TY and SX intervals, and 1.90×10^5 km^2 in the LS plus US intervals, but coals disappeared in the SJG interval (Fig. 14). Our data collected from the original descriptions show that red beds first appeared in the LS interval (e.g. at the Songshuzhen Section, Jilin Province; Appendix 3.3), and became thicker and more widely distributed in central and northeastern NCB in the US interval (Fig. 14; Appendix 3.4). After the Permian-Triassic boundary, coal seams reappeared in the Z&E interval (Appendix 3.7 and 3.8). Both the disappearance of coal swamps and occurrence of red beds indicate changing depositional environments, affecting the preservation potential of plant fossils; the preservational windows shrank substantially as oxidized conditions increased. Thus, it is interesting that the Cisuralian wetland plants in the NCB experienced a similar extinction process to the Pennsylvanian floras in Europe and North America, although the NCB extinction occurred much later.

Conifers are associated with more seasonally dry climate than Cordaitaleans, which occupied seasonal but relatively humid environments (DiMichele et al., 2001; DiMichele, 2014). It is estimated that there are ca. 20% advanced gymnosperms (including Cordaitopsida, Coniferophyta, Cycadophyta and Ginkgophyta-type leaves, petrified woods and reproductive organs and seeds) in the plant assemblages through the TY-to-US intervals in the NCB. *Cordaites* and *Cordaianthus* occurred in wide areas during these four intervals, and many possible cordaitelean leaves such as *Zamiopteris* and *Nephropsis* are found in the US interval (Li et al., 1995; Yang, 2006; Wang, 2012;

Wang ZX et al., 2016). The conifer *Walchia piniformis* was reported in the SX interval in Gansu Province, in the western part of the NCB (Liu and Shen, 1978), and another conifer, *Batenburgia*, was reported in the SX interval in Henan Province, in the southern part of the NCB (Hilton and Geng, 1998). Although no conifer leaves were found in the TY interval, the petrified conifer woods *Araucarioxylon*, *Sinopalaeospiroxylon*, *Damudoxylon*, *Decoroxylon*, *Szeioxylon*, and *Zalesskioxylon* were reported from Inner Mongolia and Liaoning (Zhang et al., 2006a). These taxa occurred later than the Carboniferous conifers of Euramerica (DiMichele et al., 2006). *Walchia* and *Ullmannia* persisted through the SX interval to the SJG interval, with more species in the US and SJG intervals over wide areas in the NCB (Wang and Wang, 1986; Li et al., 1995; Yang, 2006). Only a small number of conifers occurred in the TY-to-US intervals, probably representing pulses of slight seasonal dry climate in the overall humid wetland landscapes in the NCB. However, diverse Cordaitaleans of the US interval mostly disappeared in the SJG interval, while more coniferous leaves and petrified woods persisted in the SJG interval (Wang ZQ, 1985; Wang and Wang, 1986; Zhang et al., 2006a; Feng et al., 2011; Feng, 2012; Fig. 14). This gradual transition from cordaitalean to coniferalean dominance suggests a gradual drying trend in the tropics (DiMichele, 2014). Our polycohort analysis shows that some assemblages of the TY-to-US intervals persisted in the SJG interval, mainly the surviving walchian conifers, *Taeniopteris*, peltasperms and low-stature Equisetales. These assemblages indicate an overall dryland environment in a semiarid climate, similar to the Euramerica floras (Bashforth et al., 2014, their Table 1). Compared to the TY-to-US intervals, the percentage of advanced gymnosperms increased to about one half of total diversity in the SJG interval. Thus, there is a big change in floristic components from the US to SJG interval, with the majority of peat-forming plants *Lepidodendron*, *Tingia*, *Annularia* and *Lobatannularia* becoming extinct; the former interval is characterized by the dominance of moist wetlands, with occasional addition of elements of

seasonal dry climate, while the latter interval is dominated by semiarid dryland floras, with a few new species migrating or originating. The drying, and the associated drop of groundwater level, is the likely killer of most wetland plants.

5.4. Interpretation of the SJG/LJG transition event

Compared to the US/SJG transition event, the SJG/LJG extinction happened in a context of lower diversity, thus giving the impression that this later extinction was less severe than the former. However, our data show that the SJG/LJG transition event probably represents the terrestrial equivalent of the end-Permian mass extinction of marine faunas (e.g. Song et al., 2013; Shen et al., 2019a). The highest extinction rate occurs at the SJG/LJG transition, and the origination rate is also highest across the eight studied intervals, providing the highest turnover rates of plant genera and species. Almost all Permian plant species became extinct at this transition. The walchian conifers, a few Cordaitaleans and some residual woody lycopsids and sphenophytes in the SJG interval became extinct, and were replaced by new elements, such as *Pleuromeia*, and some new types of conifers and Cycadophyta (Wang, 1983; Wang and Wang, 1989; Zhang et al., 2006b; Fig. 14). In the LJG interval, our plant distribution map shows the lowest species diversity in only three patches. The continuous red-bed units became thickest in the LJG interval (Fig. 14). It can be seen from the few recorded sections, e.g. Nantianmen and Xigou-zhangjiamen sections in Henan Province, and Liulin-Wubu-Zhangjiayan Section in Shanxi and Shaanxi, that plant fossils were mainly found in the middle-lower part, and disappeared in the upper part of the SJG interval (Appendix 3.5). Plant fossils were not seen in the lower part of the LJG interval and reappeared as new elements in the middle-upper part of this interval in the Peijiashan Section in Shanxi Province and Yangshugou Section in Liaoning Province (Appendix 3.6), suggesting that the most severe extinction occurred between the upper part of the SJG interval and lower part of the LJG interval.

This seems to be synchronous with the negative excursion in $\delta^{13}C$ and $\delta^{18}O$ of soil carbonate in the uppermost Sunjiagou Formation and the rapid transition from meandering rivers to braided rivers and aeolian systems in the NCB (Zhu et al., 2019). Besides, it is reported that microbially-induced sedimentary structures such as wrinkles are diverse in the Liujiagou Formation (Chu et al., 2015). Similar sudden sedimentary changes in terrestrial depositional systems also happened in Russia, South Africa, Australia and Spain, as a worldwide event at the Permian-Triassic transition (Newell et al., 1999; Ward et al., 2005; Benton and Newell, 2014).

Around the PTB, there was a climate gradient from high latitudes to equatorial regions (Benton and Newell, 2014, their fig. 3; Zhu et al., 2019, their fig. 1), and thus it is not surprising that plants located in different latitudes or different regions show distinct changes. Peat mire ecosystems suddenly collapsed, with more than ca. 95% coal-bearing plants becoming extinct, in eastern Australia, which was located at high latitudes with a cold climate (Michaelsen, 2002). A similar rapid disaster of peat-forming plants also happened across the PTB in southwestern China, which was near the equator with a tropical climate (Yu et al., 2015; Feng et al., 2020). In contrast, Europe, on the other hand, which was located at low to middle latitudes with a subtropical arid climate, and peat swamps bearing abundant peat-forming plants occurred mainly in the Late Carboniferous, and disappeared in the Early Permian, along with the huge climate change from wetland to dryland (DiMichele, 2014; Cleal, 2018). Plant diversity remained very low from Guadalupian to Early Triassic in Euramerica (Rees, 2002). The extinction of peat-forming plants happened in the US/SJG interval in the NCB, earlier than in eastern Australia and southwestern China, but later than in Euramerica. However, as discussed above, in the NCB, the largest turnover event which saw the extinction of ca. 95% of the species and the origination of 90% of the species happened at the SJG/LJG transition. Plant extinction rates through the SJG/LJG transition event in the NCB are comparable to those across the coeval PTB in South China (Xiong and Wang, 2011).

This extinction was probably related to extreme heating, drought, and acid rain, which caused mass wasting of the land surface and reduced the habitable land area (Benton, 2018). Considering the overall poorer fossil preservation in drylands than in humid wetlands, the true plant extinction across the SJG/LJG transition in the NCB might have been greater. The two dramatic changes of land plants in the US/SJG and the SJG/LJG intervals, caused a ca. 8 Ma coal gap in the NCB which lasted through the SJG to HSG intervals.

6. Summary

(1) Based on an updated database, our analyses quantify the diversity change of vascular plants through the Permian to Middle Triassic in the NCB, using a hierarchy of diversity measures, bed-scale, landscape-scale and regional-scale, as explored in Cleal et al. (2012). For each of the studied intervals, we selected well-studied, representative sections, and collected from the original literature, bed by bed, data on bed thickness, lithology, and plant species in each section. Our bed-scale diversities refer to plant species from a mudstone/siltstone bed normally less than or about 10 m in thickness, or a bed of sandstone, approximately the local-scale diversity of Cleal et al. (2012). For each interval, nearby localities with comparable lithological sequences indicating deposition in a single fluvial, coastal, or deltaic system, were grouped to form a geographic patch, usually 10^4–10^5 km^2 in area. Genus and species numbers for each patch of each interval were analysed, representing landscape-scale diversity. Diversity across the whole NCB, ca. 2.70×10^6 km^2 in area, represents regional-scale diversity.

(2) The floras of the TY, SX, LS and US intervals (TY-to-US floras) in the NCB are mainly preserved in coal-forming environments. The mean bed-scale species richness of the TY-to-US floras is 8–13, but plants within an individual bed range from one to over 50 species, indicating great heterogeneity. The bed-scale diversity of the TY-to-US floras in the NCB is comparable to the local-scale diversity of the Pennsylvanian floras of the eastern part of the South Wales Coalfield. The landscape-scale species richness in the TY interval is estimated as 48 on average, while that of the SX, LS and US intervals ranges from 116–128. Polycohort analysis shows higher survival rates, with more than half of genera surviving, at the TY/SX, SX/LS, and LS/US interval transitions. The comparable diversity, higher survival rates, and relatively stable extinction, origination, and turnover rates, indicate that floras through the TY-to-US intervals are relatively continuous and stable.

(3) The US/SJG transition saw the largest diversity loss at regional scale, with high species extinction rate (94%), low origination rate (65%), and the lowest species survival percentages (< 10%) of all transitions, indicating a severe extinction event. At this time, coal swamps disappeared, the most widespread genera became extinct or shrank in geographic distribution, red beds became common, and plants consisted of the surviving walchian conifers, *Taeniopteris*, peltasperms and low-stature Equisetales, indicating an overall dryland environment. Across this transition, the fall in bed-scale and landscape-scale diversities was substantial, but not statistically significant. The drying and associated drop in groundwater level was the probable killer of most wetland plants.

(4) The SJG/LJG transition event is characterized by the highest species extinction rate (95%) and the highest origination rate (90%), leading to the highest level of turnover rates of plant genera and species. Almost all Permian plant species became extinct at this transition, and were replaced by new elements, such as *Equisetites*, *Pleuromeia*, *Voltzia*, and some new types of Cycadophyta. Plant records show that the most severe extinction occurred between the upper part of the SJG interval and lower part of the LJG interval. This event can be considered the terrestrial equivalent of the marine end-Permian mass extinction. Similar sudden sedimentary changes in terrestrial depositional system also happened in Russia, South Africa, Australia and Spain, as a worldwide event at the Permian-Triassic transition.

Declaration of competing interest

The authors declare that they have no known competing financial interests or personal relationships that could have appeared to influence the work reported in this paper.

Acknowledgements

This work was supported by the National Natural Science Foundation of China (Grants: 41802008, 41722201), the Second Tibetan Plateau Scientific Expedition (STEP) program 2019QZKK0704, and the UK Natural Environment Research Council's Eco-PT project (NE/P01377224/1). B.C.M. thanks the support provided by supported by ANR EARTHGREEN project (ANR-20-CE01-0002-01). An earlier version of the database of fossil record of Palaeozoic

vascular plants from China was constructed by the senior author (C.H.X.), under the supervision of Drs. Qi Wang and Deming Wang, who are gratefully acknowledged.

Appendixes. Supplementary data

Supplementary data to this article can be found online at http://xxx

References

Bashforth, A.R., Cleal C.J., Gibling M.R., Falcon-Lang H.J., Miller R.F., 2014. Paleoecology of Early Pennsylvanian vegetation on a seasonally dry tropical landscape (Tynemouth Creek Formation, New Brunswick, Canada). Rev. Palaeobot. Palynol. 200, 229–263.

Bambach, R.K., 2006. Phanerozoic biodiversity mass extinctions. Annu. Rev. Earth Planet. Sci. 34, 127–55.

Benton, M.J., 2009. The Red Queen and the Court Jester: species diversity and the role of biotic and abiotic factors through time. Science 323, 728–732.

Benton, M.J., 2001. Biodiversity on land and in the sea. Geol. J. 36, 211–230.

Benton, M.J., 2010. The origins of modern biodiversity on land. Phil. Trans. R. Soc. B. 365, 3667–3679.

Benton, M.J., 2018. Hyperthermal-driven mass extinctions: killing models during the Permian–Triassic mass extinction. Phil. Trans. R. Soc. A 376, 20170076.

Benton, M.J., Newell, A.J., 2014. Impacts of global warming on Permo-Triassic terrestrial ecosystems. Gondwana Res. 25, 1308–1337.

Benton, M.J., Ruta, M., Dunhill, A.M., Sakamoto, M., 2013. The first half of tetrapod evolution, sampling proxies, and fossil record quality. Palaeogeogr. Palaeoclimatol. Palaeoecol. 372, 18–41.

Bond, D.P., Hilton, J., Wignall, P.B., Ali, J.R., Stevens, L.G., Sun, Y., Lai, X., 2010. The Middle Permian (Capitanian) mass extinction on land and in the oceans. Earth-Sci. Rev. 102, 100–116.

Boucot, A.J., Chen, X., Scotese, C.R., Morley, R.J., 2013. Phanerozoic Paleoclimate: An Atlas of Lithologic Indicators of Climate. SEPM Society for Sedimentary Geology, Tulsa.

Calder, J.H., Gibling, M.R., 1994. The Euramerican Coal Province: controls on Late Paleozoic peat accumulation. Palaeogeogr. Palaeoclimatol. Palaeoecol. 106, 1–21.

Cascales-Miñana, B., 2016. Apparent changes in the Ordovician–Mississippian plant diversity. Rev. Palaeobot. Palynol. 227, 19–27.

Cascales-Miñana, B., Cleal, C.J., Diez, J.B., 2013. What is the best way to measure extinction? A reflection from the palaeobotanical record. Earth-Sci. Rev. 124, 126–147.

Cascales-Miñana, B., Muñoz-Bertomeu, J., Ros, R., Segura, J., 2010. Trends and patterns in the evolution of vascular plants: implications of a multilevel taxonomic analysis. Lethaia, 43, 545–557.

Cascales-Miñana, B., Servais, T., Cleal, C.J., Gerrienne, P., Anderson, J., 2018. Plants—the great survivors! Geol. Today 34, 224–229.

Chu, D.L., Tong, J.N., Song, H.J., Benton, M.J., Bottjer, D.J, Song, H.Y., Li, T., 2015. Early Triassic wrinkle structures on land: stressed environments and oases for life. Sci. Rep. 5, 10109.

Cleal, C.J., 2018. The Carboniferous coal swamp floras of England: a window on an ancient tropical ecosystem. P. Geologist Assoc. 129, 329–351.

Cleal, C.J., Cascales-Miñana, B., 2014. Composition and dynamics of the great Phanerozoic Evolutionary Floras. Lethaia 47, 469–484.

Cleal, C.J., Cascales-Miñana, B., 2021. Evolutionary floras – revealing large–scale patterns in Palaeozoic vegetation history. Jl Palaeosci. 70, 31–42.

Cleal, C.J., Thomas, B.A., in press. Naming of parts: the use of fossil-taxa in palaeobotany. Fossil Imprint 77.

Cleal, C.J., Wang, Z.Q., 2002. A new and diverse plant fossil assemblage from the upper Westphalian Benxi Formation, Shanxi, China, and its palaeofloristic significance. Geol. Mag. 139, 107–130.

Cleal, C.J., Uhl, D., Cascales-Miñana, B., Thomas, B.A., Bashforth, A.R., King, S.C., Zodrow, E.L., 2012. Plant biodiversity changes in Carboniferous tropical wetlands. Earth-Sci. Rev. 114, 124–155.

Cleal, C.J., Pardoe, H.S., Berry, C.M., Cascales-Miñana, B., Davis, B.A.S., Diez, J.B., Filipova-Marinova M.V., Giesecke, T., Hilton, J., Ivanov, D., Kustatscher, E., Leroy, S.A.G., McElwain, J.C., Opluštil, S., Popa M.E., Seyfullah, L.J., Stolle, E., Thomas, B.A., Uhl, D., 2021. Palaeobotanical experiences of plant diversity in deep time. 1: How well can we identify past plant diversity in the fossil record? Palaeogeogr. Palaeoclimatol. Palaeoecol. https://doi.org/10.1016/j.palaeo.2021.110481

Di Marco, M.D., Brooks, T., Cuttelod, A., Fishpool, L.D.C., Rondinini, C., Smith, R.J., Bennun, L., Butchart, S.H.M., Ferrier, S.F., Foppen, R.P.B., Joppa, L., Juffe-Bignoli, D., Knight, A.T., Lamoreux, J.F., Langhammer, P.F., May, I., Possingham, H.P., Visconti, P., Watson, J.E.M., Woodley, S., 2016. Quantifying the relative irreplaceability of important bird and biodiversity areas. Conserv. Biol. 30, 392–402.

DiMichele, W.A., 2014. Wetland-dryland vegetational dynamics in the Pennsylvanian ice age tropics. Int. J. Plant Sci. 175, 123–164.

DiMichele, W.A., Nelson, W.J., 1989. Small-scale spatial heterogeneity in Pennsylvanian-age vegetation from the roof shale of the Springfield Coal (Iillinois Basin). Palaios, 4, 276–280.

DiMichele, W.A., Pfefferkorn H.W., Gastaldo, R.A., 2001. Response of Late Carboniferous and Early Permian plant communities to climate change. Annu. Rev. Earth Planet. Sci 29: 461–487.

DiMichele, W.A., Tabor, N.J., Chaney, D.S., Nelson, W.J., 2006. From wetlands to wet spots: Environmental tracking and the fate of Carboniferous elements in Early Permian tropical

floras. In: Greb, S.F., DiMichele, W.A. (Eds.) Wetlands through time: Geological Society of America Special Paper 399, pp. 223–248.

Dyer, E.E., Cassey, P., Redding, D.W., Collen, B., Franks, V., Gaston, K.J., Jones, K.E., Kark, S., Orme, C.D.L., Blackburn, T.M., 2017. The global distribution and drivers of alien bird species richness. PLoS Biol. 15, e2000942.

Fan, J.X., Shen, S.Z., Erwin, D.H., Sadler, P.M., MacLeod, N., Cheng, Q.M., Hou, X.D., Yang, J., Wang, X.D., Wang, Y., Zhang, H., Chen, X., Li, G.X., Zhang, Y.C., Shi, Y.K., Yuan, D.X., Chen, Q., Zhang, L.N., Li, C., Zhao, Y.Y., A high-resolution summary of Cambrian to Early Triassic marine invertebrate biodiversity. Science 367, 272–277.

Feng, Z., 2012. *Ningxiaites specialis*, a new woody gymnosperm from the uppermost Permian of China. Rev. Palaeobot. Palynol. 181, 34–46.

Feng, Z., Wang, J., Rößler, R., 2011. A unique gymnosperm from the latest Permian of China, and its ecophysiological implications. Rev. Palaeobot. Palynol. 165, 27–40.

Feng, Z., Wei, H.B., Guo, Y., He, X.Y., Sui, Q., Zhou, Y., Liu, H.Y., Gou X.D., Lv, Y., 2020. From rainforest to herbland: new insights into land plant responses to the end-Permian mass extinction. Earth-Sci. Rev. 204, 103153.

Galtier, J., 1997. Coal-ball floras of the Namurian-Westphalian of Europe. Rev. Palaeobot. Palynol. 95, 51–72.

Galtier, J., Daviero, V., 1999. Structure and development of *Sphenophyllum oblongifolium* from the Upper Carboniferous of France. Int J Plant Sci. 160, 1021–1033.

Gastaldo, R.A., 1985. Upper Carboniferous paleoecological reconstructions: observations and reconsiderations. In: Compte rendu 10e Congrès International de Stratigraphie et de Géologie du Carbonifère, Volume 2. Inst. Geologico y Mineiro de España, Madrid, pp. 281–296.

Gastaldo, R.A., Demko, T.M., 2011. The relationship between continental landscape evolution and the plant-fossil record: long term hydrologic controls on preservation (Chapter 7). In: Allison, P.A., Bottjer, D.J. (Eds.) [Topics in Geobiology] Taphonomy: Process and bias through time. 32, pp. 249–285.

Gastaldo, R.A., DiMichele, W.A., Pfefferkorn, H.W., 1996. Out of the icehouse into the greenhouse: A Late Paleozoic analog for modern global vegetational change. GSA Today, 6, 1–7.

Gastaldo, R.A., Pfefferkorn, H.W., DiMichele, W.A., 1995, Taphonomic and sedimentologic characterization of ‘‘roof-shale’’ floras. In: Lyons, P., (Ed.), Historical perspective of early twentieth century Carboniferous paleobotany in North America. Geological Society of America Memoir 185, pp. 341–352.

Geiger, R., Aron, R.H., Todhunter, P., 2009. The climate near the ground. Rowman & Littlefield, Lanham, MD.

Gu, Zhi, 1974. “Palaeozoic Plants from China” Writing Group of Nanjing Institute of Geology and Palaeontology, Institute of Botany, Academia Sinica. Palaeozoic Plants from China. Science Press, Beijing. (in Chinese)

Halle, T.G., 1927. Palaeozoic plants from central Shansi. Palaeontologia Sinica Series A, 2.

Hammer, Ø., Harper, D.A.T., Ryan, P.D., 2001. PAST: Paleontological statistics software package for education and data analysis. Palaeontol. Electron. 4: 1–9.

Harper, D.A.T., Servais, T., 2018. Contextualizing the onset of the Great Ordovician Biodiversification Event. Lethaia 51, 149–150.

He, X.L., Zhang, Y.J., Zhu, M.L., Zhang, G.Y., Zhuang, S.J., Zeng, Y., Song, P., 1990. Research on the Late Palaeozoic coal-bearing stratigraphy and biota in Junggar, Nei Mongol (Inner Mongolia). China Mining and Technology University Publishing House, Xuzhou. (in Chinese with English summary)

Hilton, J., Cleal, C.J., 2007. The relationship between Euramerican and Cathaysian tropical floras in the Late Palaeozoic: Palaeobiogeographical and palaeogeographical implications. Earth-Sci. Rev. 85, 85–116.

Hilton, J., Geng, B.Y., 1998. *Batenburgia sakmarica* Hilton et Geng, gen. et sp. nov., a new genus of conifer from the Lower Permian of China. Rev. Palaeobot. Palynol. 103, 263–287.

Hofmann, R., Hautmann, M., Bucher, H., 2017. Diversity partitioning in Permian and Early Triassic benthic ecosystems of the Western USA: a comparison. Hist. Biol. 29, 918–930.

Huang, B., Jin, J.S., Rong, J.Y., 2018. Post-extinction diversification patterns of brachiopods in the early–middle Llandovery, Silurian. Palaeogeogr. Palaeoclimatol. Palaeoecol. 493: 11–19.

Huang, B.C., Yan, Y.G., Piper, J.D.A., Zhang, D.H., Yi, Z.Y., Yu, S., Zhou, T.G., 2018. Paleomagnetic constraints on the paleogeography of the East Asian blocks during Late Paleozoic and Early Mesozoic times. Earth-Sci. Rev. 186, 8–36.

Isbell, J.L., Miller, M.F., Wolfe, K.L., Lenaker, P.A., 2003. Timing of late Paleozoic glaciation in Gondwana: Was glaciation responsible for the development of northern hemisphere cyclothems? In: Chan, M.A., Archer, A.W. (Eds.) Extreme depositional environments: Mega end members in geologic time: Boulder, Colorado, Geological Society of America Special Paper 370, pp. 5–24.

Jin, Y.G., Shang, Q.H., Hou, J.P., Li L., Wang, Y.J., Zhu, Z.L., Fei, S.Y., 2000. Chinese stratigraphic code of Permian. Geological Publishing House, Beijing. (in Chinese)

Kiel, S., 2017. Using network analysis to trace the evolution of biogeography through geologic time: A case study. Geology 45, 711–714.

Knoll, A.H., Niklas, K.J. Tiffney, B.H., 1979. Phanerozoic land-plant diversity in North America. Science 206, 1400–1402.

Kolasa, J.; Rollo, C.D., 1991. Introduction: The heterogeneity of heterogeneity: A glossary (Chapter 1). In: Kolasa, J., Pickett, S.T.A. (Eds.) [Ecological Studies] Ecological heterogeneity. 86, pp. 1–23.

Li, X.X., Zhou, Z.Y., Cai, C.Y., Sun, G., Ouyang, S., Deng, L.H., 1995. Fossil floras of China through the geological ages. Guangdong Science and Technology Press, Guangzhou. (in Chinese and English)

Liu, G.H., 1990. Permo-Carboniferous paleogeography and coal accumulation and their tectonic control in the North and South China continental plates. Int. J. Coal Geol. 16, 73–117.

Liu, J., 2018. New progress on the correlation of Chinese terrestrial Permo-Triassic strata. Vertebrata PalAsiatica 56, 327–342. (in Chinese with English summary)

Liu, H.C., Shen, G.L., 1978. On the occurrence of *Walchia piniformis* in China for the first time and the description of *W. longifolia* sp. nov. J. Lanzhou Univ. (Nat. Sci.) 2, 136–144. (in Chinese with English abstract)

Liu, F., Zhu, H.C., Ouyang, S., 2015. Late Pennsylvanian to Wuchiapingian palynostratigraphy of the Baode section in the Ordos Basin, North China. J. Asian Earth Sci. 111, 528–552.

Liu, J., Ramezani, J., Li, L., Shang, Q.H., Xu, G.H., Wang Y.Y., Yang J.S., 2018. High-precision temporal calibration of Middle Triassic vertebrate biostratigraphy: U-Pb zircon constraints for the *Sinokannemeyeria* Fauna and *Yonghesuchus*. Vertebrata PalAsiatica 56, 16–24.

Lu, J., Zhou, K., Yang, M., Zhang, P., Shao, L., Hilton, J., 2021. Records of organic carbon isotopic composition ($\delta 13C_{org}$) and volcanism linked to changes in atmospheric pCO_2 and climate during the Late Paleozoic Icehouse. Global and Planetary Change 207, p.103654.

Magurran, A.E., 2004. Measuring Biological Diversity. Wiley-Blackwell, Oxford.

Michaelsen, P., 2002. Mass extinction of peat-forming plants and the effect on fluvial styles across the Permian-Triassic boundary, northern Bowen Basin, Australia. Palaeogeogr. Palaeoclimatol. Palaeoecol. 179, 173–188.

Newell, A.J., Tverdokhlebov, V.P., Benton, M.J., 1999 Interplay of tectonics and climate on a transverse fluvial system, Upper Permian, southern Uralian foreland basin, Russia. Sed. Geol. 127, 11–29.

Nichos, G., 2009. Sedimentology and stratigraphy. Wiley-Blackwell publication, London UK.

Niklas, K.J., Tiffney, B.H., 1994. The quantification of plant biodiversity through time. Phil. Trans. R. Soc. Lond. B. 345, 35–44.

Pardoe, H.S., Cleal, C.J., Berry, C.M., Cascales-Miñana, B., Davis, B.A.S., Diez, J.B., Filipova-Marinova M.V., Giesecke, T., Hilton, J., Ivanov, D., Kustatscher, E., Leroy, S.A.G., McElwain, J.C., Opluštil, S., Popa M.E., Seyfullah, L.J., Stolle, E., Thomas, B.A., Uhl, D., 2021. Palaeobotanical experiences of plant diversity in deep time. 2: How to measure and analyse past plant biodiversity. Palaeogeogr. Palaeoclimatol. Palaeoecol. https://doi.org/10.1016/j.palaeo.2021.110618.

Pfefferkorn, H.W., Wang, J., 2007. Early Permian coal–forming floras preserved as compressions from the Wuda District (Inner Mongolia, China). Int. J. Coal Geol. 69: 90–102.

Raup, D.M., Sepkoski, J.J., JR., 1982. Mass extinctions in the marine fossil record. Science 215, 1501–1503.

Rees, P.M., 2002. Land-plant diversity and the end-Permian mass extinction. Geology 30, 827–830.

Sepkoski, J.J., JR., 1979. A kinetic model of Phanerozoic taxonomic diversity II. Early Phanerozoic families and multiple equilibria. Paleobiology 5, 222–251.

Scotese, C.R., 2001. Atlas of Earth History. Paleogeography, PALEOMAP Project vol. 1 (http:www.scotese.com). Arlington, TX.

Shen, G.L., Wang, J., Liu, H.Q., 1997. On succession of Permian floras in North Qilian area. Acta Geologica Gansu. 6, 52–63.

Shen, S.Z., Crowley, J.L., Wang, Y., Bowring, S.A., Erwin, D.H., Sadler, P.M., Cao, C.Q., Rothman, D.H., Henderson, C.M., Ramezani, J., Zhang, H., Shen, Y.N., Wang, X.D., Wang, W., Mu, L., Li, W.Z., Tang, Y.G., Liu, X.L., Liu, L.J., Zeng, Y., Jiang, Y.F., Jin, Y.G., 2011. Calibrating the end-Permian mass extinction. Science 334, 1367–1372.

Shen, Z.X., Törnqvist, T., E., Mauz, B., Chamberlain, E.L., Nijhuis, A.G., Sandoval, L., 2015. Episodic overbank deposition as a dominant mechanism of floodplain and delta-plain aggradation. Geology 43, 875–878.

Shen, S.Z., Ramezani, J., Chen, J., Cao, C.Q., Erwin, D.H., Zhang, H., Xiang, L., Schoepfer, S.D., Henderson, C.M., Zheng, Q.F., Bowring, S.A., Wang, Y., Li, X.H., Wang, X.D., Yuan, D.X., Zhang, Y.C., Mu, L., Wang, J., Wu, Y.S., 2019a. A sudden end-Permian mass extinction in South China. Geol. Soc. Am. Bull. 131, 205–223.

Shen, S.Z., Zhang, H., Zhang, Y.C., Yuan, D.X., Chen, B., He, W.H., Mou, L., Lin, W., Wang, W.Q., Chen, J., Wu, Q., Cao, C.Q., Wang Y., Wang, X.D., 2019b. Permian integrative stratigraphy and timescale of China. Sci. China Earth Sci., 62: 154–188.

Song, H.J., Wignall, P.B., Tong, J.N., Yin, H.F., 2013. Two pulses of extinction during the Permian–Triassic crisis. Nat. Geosci. 6, 52–56.

Stevens, L.G., Hilton, J., Bond, J.H.D., 2011. Radiation and extinction patterns in Permian floras from North China as indicators for environmental and climate change. J. Geol. Soc. London 168, 607–619.

Thomas, B.A., 2007. Phytogeography of Asturian (Westphalian D) lycophytes throughout the Euramerican belt of coalfields. Geol. Mag. 144, 457–463.

Thomas, B.A., Cleal, C.J., 2017. Distinguishing Pennsylvanian-age lowland, extra-basinal and upland vegetation. Palaeobio. Palaeoenv. 97, 273–293.

Thomas, B.A., Seyfullah, L.J., 2015. *Stigmaria* Broungniart: a new specimen from Duckmantian (Lower Pennsylvanian) Brymbo (Wrexham, North Wales) together with a review of known casts and how they were preserved. Geol. Mag. 152, 858–870.

Valdés, A., Lenoir, J., Gallet-Moron, E., Andrieu, E., Brunet, J., Chabrerie, O., Closset-Kopp, D., Cousins, S.A.O., Deconchat, M., De Frenne, P., De Smedt, P., Diekmann, M., Hansen, K., Hermy, M., Kolb, A., Liira, J., Lindgren, J., Naaf, T., Paal, T., Prokofieva, I., Scherer-Lorenzen, M., Wulf, M., Verheyen, K., Decocq, G., 2015. The contribution of patch-scale conditions is greater than that of macroclimate in explaining local plant diversity in fragmented forests across Europe. Global Ecol. Biogeogr. 24, 1094–1105.

Wang, Z.Q., 1983. New data of fossil plants from Shiqianfeng Group in N. China. Bull. Geol. Soc. Tianjin 1, 72–80. (in Chinese)

Wang, Z.Q., 1985. Palaeovegetation and plate tectonics: palaeophytogeography of North China during Permian and Triassic times. Palaeogeogr. Palaeoclimatol. Palaeoecol. 49, 25–45.

Wang, Z.Q., 1989. Permian gigantic palaeobotanical events in North China. Acta Palaeontol. Sin. 28, 314–343. (in Chinese with English summary)

Wang, R.N., 1997. New advance of the study of the Shiqianfeng Formtion in western Henan. Geol Rev. 43, 200–209. (in Chinese with English abstract)

Wang, J., 2010. Late Paleozoic macrofloral assemblages from Weibei Coalfield, with reference to vegetational change through the Late Paleozoic Ice-age in the North China Block. Int. J. Coal Geol. 83, 292–317.

Wang, J., Pfefferkorn, H.W., 2013. The Carboniferous–Permian transition on the North China microcontinent—Oceanic climate in the tropics. Int. J. Coal Geol. 119, 106–113.

Wang, Q., Huang, B., 2020. Network analysis and its application in paleontology—a preliminary introduction. Acta Palaeontol. Sin. 59(3), 380–392. (in Chinese with English summary)

Wang, Z.Q., Wang, L.X., 1986. Late Permian fossil plants from the lower part of the Shiqianfeng (Shichienfeng) Group in North China. B. Tianjin Inst. Geology Miner. Resour. Chin. Acad. Geol. Sci. 15, 1–80. (in Chinese with English summary)

Wang, Z.Q., Wang, L.X., 1989. Earlier Early Triassic fossil plants from upper part of the Shiqianfeng Group in North China. Shanxi Geology 4, 23–40. (in Chinese with English abstract)

Wang, Z.Q., Wang, L.X., 1990a. A new plant assemblage from the bottom of the Mid-Triassic Ermaying Formation. Shanxi Geology 5, 303–318. (in Chinese with English abstract)

Wang, Z.Q., Wang, L.X., 1990b. Late Early Triassic fossil plants from upper part of the Shiqianfeng Group in North China. Shanxi Geology 5, 97–154. (in Chinese with English summary)

Wang, S.J., Tian, B.L., Chen, G.R., 2002a. Anatomically preserved lepidodendralean plants from Permian coal balls of China: leaves of *Lepidophylloides* Snigirevskaya. Rev. Palaeobot. Palynol. 122, 63–76.

Wang, S.J., Tian, B.L., Chen, G.R., 2002b. Anatomically-preserved Lepidodendralean plants from Permian coal balls of China: *Sigillariopsis* Scott. Acta Bot. Sin. 44, 104–112.

Wang, J., Pfefferkorn, H.W., Zhang, Y., Feng, Z., 2012. Permian vegetational Pompeii from Inner Mongolia and its implications for landscape paleoecology and paleobiogeography of Cathaysia. Proc. Natl. Acad. Sci. U. S. A. 109, 4927–4932.

Wang, Z.X., Sun, B.N., Wang, X.L., Chen, Y.Q., Sun, F.K., Xiong, C.H., 2016. A new cordaitean pollen cone and pollen grains *in situ* from the Early Permian of Hexi Corridor and its geotectonic significance. Palaeogeogr. Palaeoclimatol. Palaeoecol. 463, 261–274.

Wang, F., Chen, R., Liang, Q.S., Chang, X.L., Tian, J.C., Deng, X.Q., 2019. Geochemical characteristics and depositional environments of mudstones from the Triassic Zhifang Formation in the Tongchuan Area, southern Ordos Basin, China. Geol J. 55, 3857–3869.

Wang, J., Hilton, J., Pfefferkorn H.W., Wang, S.J., Zhang, Y., Bek, J., Pšenička, J., Seyfullah, L.Y., Dilcher, D., 2021. Ancient noeggerathialean reveals the seed plant sister group

diversified alongside the primary seed plant radiation. Proc. Natl. Acad. Sci. U. S. A. 118, No. 11 e2013442118.

Ward, P.D., Botha, J., Buick, R., De Kock, M.O., Erwin, D.H., Garrison, G.H., Kirschvink, J.L., Smith, R., 2005. Abrupt and gradual extinction among Late Permian land vertebrates in the Karoo Basin, South Africa. Science 307, 709–714.

Whittaker, R.J., Willis, K.J., Field, R., 2001. Scale and species richness: towards a general, hierarchical theory of species diversity. J. Biogeogr. 28, 453–470.

Wu, Q., Ramezani, J., Zhang, H., Wang, J., Zeng, F.G., Zhang, Y.C., Liu, F., Chen, J., Cai, Y.F., Hou, Z.S., Liu, C., Yang, W., Henderson, C.M., Shen, S.Z., 2021. High-precision U-Pb age constraints on the Permian floral turnovers, paleoclimate change, and tectonics of the North China block. Geology. https://doi.org/10.1130/G48051.1

Xiong, C.H., Wang, Q., 2011. Permian–Triassic land–plant diversity in South China: was there a mass extinction at the Permian/Triassic boundary? Paleobiology 37, 157–167.

Xue, J.Z., Huang, P., Wang, D.M., Xiong, C.H., Liu, L., Basinger, J.F., 2018. Silurian-Devonian terrestrial revolution in South China: Taxonomy, diversity, and character evolution of vascular plants in a paleogeographically isolated, low-latitude region. Earth-Sci. Rev. 180, 92–125.

Yang, G.X., 2006. The Permian Cathaysian flora in western Henan Province, China—Yuzhou Flora. Geological Publishing House, Beijing. (in Chinese and English)

Yang, G.X., Wang, H.S., 2012. Yuzhou Flora—A hidden gem of the Middle and Late Cathaysian Flora. Sci. China. Earth. Sci. 55, 1601–1619.

Yu, J., Broutin, J., Chen, Z.Q., Shi, X., Li, H., Chu, D.L., Huang, Q.S., 2015. Vegetation changeover across the Permian–Triassic Boundary in Southwest China. Earth-Sci. Rev. 149, 203–224.

Zhang, W., Zheng, S.L., Li, Y., Li, N., 2006a. Carboniferous—Permian petrified woods. In: Shenzhen municipal administration, Shenzhen Fairy Lake Botanical Garden, Ministry of Land and Resources (eds.) Petrified woods in China. China Forestry Press, Beijing. Pp. 33–100. (in Chinese)

Zhang, W., Li, N., Zheng, S.L., Fu, X.P., 2006b. Triassic petrified woods. In: Shenzhen municipal administration, Shenzhen Fairy Lake Botanical Garden, Ministry of Land and Resources eds. Petrified woods in China. China Forestry Press, Beijing. Pp. 101–119. (in Chinese)

Zhu, Z.C., Liu, Y.Q., Kuang, H.W., Benton, M.J., Newell, A.J., Xu, H., An, W., Ji, S.A., Xu, S.C., Peng, N., Zhai, Q.G., 2019. Altered fuvial patterns in North China indicate rapid climate change linked to the Permian-Triassic mass extinction. Sci. Rep. 9, 16818.

Figure legends

Fig. 1. Palaeogeographic map showing the location of the North China Block (NCB) in the Permian (A, modified from Huang et al., 2018), and the division of the NCB into four subregions based on Permian lithostratigraphy (B, based on Jin et al., 2000). The NCB was reconstructed as occupying a low-latitude position through the Permian to Middle Triassic in Huang et al. (2018), while in other schemes it is located further north than 30ºN during the Early and Middle Triassic (Scotese, 2001; Boucot et al., 2013). MOB, NCB, SCB, NQ, SQ, IC, and Si indicate the Mongolian, North China, South China, North Qiangtang, South Qiangtang, Indochina, and Sibumasu blocks, respectively.

Fig. 2. Correlation and suggested age model of typical plant-bearing formations across the four subregions in the NCB through the Cisuralian to Middle Triassic, based on various sources. Fm., Formation. It should be noted that the correlation of the Permian strata of the NCB to the standard international chronostratigraphic stages remains much debated, and different schemes have been suggested by different authors (e.g. Hilton and Cleal, 2007; Wang, 2010; Liu, 2018; Shen et al., 2019; Wu et al., 2021; Lu et al., 2021). For instance, Wu et al. (2021) demonstrated a ca. 20-myr-hiatus between the Upper Shihhotse and Sunjiagou formations. Suggested correlations of other lithostratigraphic units that have a restricted distribution in the NCB are introduced in Appendix 1.

Fig. 3. Schematic diagram showing the hierarchy of regional-scale, landscape-scale, and bed-scale diversity of plant macrofossils. A. Regional-scale diversity is defined to represent the diversity across the whole (palaeo)continent, which shows diverse depositional environments with plant fossils; landscape-scale diversity, to represent the diversity of a local area within the same depositional system, such as a deltaic system (left inset); bed-scale diversity, to represent the diversity from an individual bed (right inset). The summary diagram of continental environments is modified from Figure 5.13 of Nichols (2009). B. Suggested temporal scale and geographical scale of the different diversity metrics (cf. Benton, 2009, his Figure 1A). The geographical scale is similar to that suggested by Cleal et al. (2012). See text for details.

Fig. 4. Cross plot of bed thickness and bed-scale species richness (S_{bed}) (A), and S_{bed} values in different individual beds (B). Data based on Table 1. Abbreviations (same as in the following figures and tables): TY, Taiyuan interval; SX, Shanxi interval; LS, Lower Shihhotse interval; US, Upper Shihhotse interval; SJG, Sunjiagou interval; LJG, Liujiagou interval; HSG, Heshanggou interval; and Z&E, Zhifang and Ermaying interval.

Fig. 5. Species distribution maps of the NCB through the eight studied intervals. For each interval, different geographic patches are recognized, based on similar stratigraphic sequence and lithological features. Representative localities with well-documented plant species and lithological

descriptions are indicated by stars; data from these localities were used for analyses of bed-scale diversity and heterogeneity among sections. Other localities/sections are indicated by dots (different colours indicate different lithological unit names used). A. TY interval, with seven patches (TY1–TY7). The Zibo locality can be considered as a further patch, which shows an area far less than other patches. B. SX interval, with seven patches (SX1–SX7). There are five other localities including Dongheishan forming a further, much smaller patch. C. LS interval, with seven patches (LS1–LS7) and four other localities forming a further, smaller one. D. US interval, with eight patches (US1–US8). E. SJG interval, with four patches (SJG1–SJG4) and one isolated locality (Shitanjing). F. LJG interval, with three patches (LJG1–LJG3). G. HSG interval, with three patches (HSG1–HSG3). H. Z&E interval, with two patches (Z&E1, Z&E2) and two isolated localities (Linjiawaizi and Qiandianzi). Species numbers in different patches is shown by different coloration (key at the foot of the figures). See text for details.

Fig. 6. Bed-scale species diversity (S_{bed}) of plant macrofossils in the NCB through the eight studied intervals. A and B at the bottom of the figure indicate two correlation schemes of the strata of the NCB to the standard international chronostratigraphic stages, along with the numerical ages of the boundaries. A, based on Wang (2010); B, based on Wu et al. (2021), who suggested that the Upper Shihhotse Formation (US) spans from ca. 294 Ma to 280 Ma and the base of the Sunjiagou Formation (SJG) is ca. 260 Ma. As, Asselian; Sa, Sakmarian; Ar, Artinskian; Ku, Kungurian; Ro, Roadian; Wo, Wordian; Ca, Capitanian; Wu, Wuchiapingian; Ch, Changhsingian; In, Induan; Ol,

Olenekian; An, Anisian; and PTB, the Permian-Triassic boundary (same in the following figures). Also see Fig. 2. For each interval, the number of species from representative fossiliferous beds were counted and then analysed. The 25–75% quartiles of species diversity from these beds are shown using a box (same in the following figures): the median value is a horizontal line inside the box; the minimal and maximum values are short horizontal lines below and above the box; circles and stars are outliers. Data based on Tables 1 and 3.

Fig. 7. Landscape-scale diversity dynamics of plant macrofossils in the NCB through the eight studied intervals. For each interval, G_{pat} (A) and S_{pat} (B) from each recognized patch were counted and then analysed. Data based on Tables 2 and 3.

Fig. 8. Correlation between genus/species numbers and patch areas for the Permian intervals. A. TY interval. B. SX interval. C. LS interval. D. US interval. Data based on Table 2.

Fig. 9. Cumulative numbers of genera (A) and species (B) in different intervals in the NCB, along with stepwise addition of different patches. Data based on Appendix 3.1–3.8.

Fig. 10. Generic Network Analysis (NA) among patches through TY to Z&E intervals. A–D. TY to US intervals. E–H. SJG to Z&E intervals. Data based on Appendix 3.1-3.8.

Fig. 11. Regional-scale diversity dynamics of genera and species of plant macrofossils in the NCB through the eight studied intervals. A. Number of total genera (= foliage genera + non-foliage genera, blue line) and species (= foliage species + non-foliage species, green line), and number of foliage genera and species only (black dotted line and solid line). B. Heterogeneity indices among sections (average and standard deviation). Data based on Appendix 2 and Table 4.

Fig. 12. Regional-scale diversity dynamics of genera and species of plant macrofossils in the NCB through the eight studied intervals. A. Extinction, origination, and turnover rates of genera. B. Extinction, origination, and turnover rates of species. Data based on Table 5.

Fig. 13. Polycohort analysis for the raw diversity of plant macrofossils in the NCB through the eight studied intervals, showing percentage of surviving genera (A) and species (B) in succeeding intervals. Arrows indicate two episodes of major declines of plant diversity, one at the US/SJG transition, and the other at the SJG/LJG transition. Data based on Table 6.

Fig. 14. Extinctions, floral components, thickness of red-beds, and areas with coal seams in the NCB through the Cisuralian to Middle Triassic. Area with >5-m-thick coal seams, estimated based on palaeomaps of Liu (1990), greatly shrank from the TY and SX intervals to the LS and US intervals and disappeared in the SJG interval. Data for the thickness of red-bed units, which are

defined here as a suite of beds with a continuous red coloration, were collected from the literature (Appendix 3.1–3.8).

Table 1. Bed-scale diversity of the eight intervals through the Permian to Middle Triassic of North China.

Interval	Formation	Section	Bed number and lithology*	Bed thickness (m)	Species richness**	References
TY	Taiyuan Fm.	Babao section	13, black shale	1.8	10	[1]
TY	Ibid.	Ibid.	11, black shale	1.9	4	[1]
TY	Ibid.	Ibid.	8, black shale	2.3	5	[1]
TY	Ibid.	Hulstai coalfield	127, black mudstone	1.8	3	[2]
TY	Ibid.	Ibid.	122, silty mudstone	5.0	3	[2]
TY	Ibid.	Ibid.	121, mudstone	1.3	9	[2]
TY	Ibid.	Fangtagou section	27, black shale	0.4	6	[3]
TY	Ibid.	Wuda Coal Mine	Flora 4, shale	0.22	22	[4, 5]
TY	Ibid.	Ibid.	Flora 3, tuff	0.2	2	[4]
TY	Ibid.	Ibid.	Flora 2, tuff	0.46	40	[4, 6]
TY	Ibid.	Ibid.	Flora 1, sandy mudstone	0.14	4	[4]
TY	Zhutun Fm.	Dafengkou section	8, mudstone, with coal	6.0	6	[7]
TY	Ibid.	Ibid.	6-1, lower: quartz sandstone; middle-upper: siltstone and mudstone	12.0	2	[7]
SX	Shanxi	Dongheish	19, mudstone	1.3	1	[8]

	Fm.	an section				
SX	Ibid.	Ibid.	16, siltstone	8.8	8	[8]
SX	Ibid.	Ibid.	10, siltstone	7.7	6	[8]
SX	Ibid.	Ibid.	3, siltstone	3.9	6	[8]
SX	Ibid.	Daquan section	12, mudstone, with coal	3.8	21	[9]
SX	Ibid.	Ibid.	8, siltstone, mudstone and black shale	3.9	12	[9]
SX	Ibid.	Ibid.	7, conglomerate with sandstone	3.9	6	[9]
SX	Ibid.	Ibid.	6, siltstone, mudstone and sandstone	3.9	14	[9]
SX	Ibid.	Shabatai section	38, sandstone and sandy mudstone	7.5	1	[10]
SX	Ibid.	Ibid.	28, mudstone and siltstone	4	2	[10]
SX	Ibid.	Ibid.	27, mudstone	10	11	[10]
SX	Ibid.	Heidaigou section	54, mudstone	3	4	[3]
SX	Ibid.	Ibid.	50, siltstone and mudstone, with coal	4.8	10	[3]
SX	Ibid.	Ibid.	46, mudstone	1.7	22	[3]
SX	Ibid.	Ibid.	42, coal	0.4	11	[3]
SX	Ibid.	Ibid.	40, sandy mudstone	3.1	40	[3]
SX	Ibid.	Ibid.	38, sandy mudstone	2.8	10	[3]
SX	Ibid.	Ibid.	35, mudstone	5	25	[3]
SX	Ibid.	Ibid.	33, sandy mudstone	1.7	29	[3]
SX	Ibid.	Ibid.	31, mudstone	0.3	24	[3]
SX	Ibid.	Longwang gou section	59, siltstone	0.7	23	[3]

SX	Ibid.	Ibid.	55, sandy mudstone	6.3	55	[3]
SX	Ibid.	Ibid.	53, sandy mudstone	2.7	1	[3]
SX	Ibid.	Ibid.	48, sandy mudstone	0.3	1	[3]
SX	Ibid.	Ibid.	47, siltstone	2.3	1	[3]
SX	Ibid.	Caotan section	57, shale	5.8	14	[1]
SX	Ibid.	Babao section	33, shale	2.3	7	[1]
SX	Ibid.	Ibid.	20, shale	2.8	5	[1]
SX	Ibid.	Guyuan Section	15, sandstone and shale	1.8	6	[1]
SX	Ibid.	Ibid.	7, shale	7.2	6	[1]
SX	Ibid.	Hesheng section	3, sandstone and sandy mudstone	10.4	23	[11]
SX	Ibid.	Ibid.	2, sandstone and mudstone	6	2	[11]
SX	Shenhou Fm.	Dafengkou section	14, sandstone and silty mudstone	9.4	7	[7]
SX	Ibid.	Ibid.	11, mudstone with coal	3.6	27	[7]
LS	Lower Shihhotse Fm.	Liuqiao section	7, mudstone and siltstone	8.1	4	[12]
LS	Ibid.	Ibid.	6, siltstone and mudstone	8.9	3	[12]
LS	Ibid.	Ibid.	4, siltstone	3.4	7	[12]
LS	Ibid.	Laojingou section	3, mudstone	0.1	9	[13]
LS	Ibid.	Hulstai section	155, siltstone	9.88	2	[14]
LS	Ibid.	Songshuzhen section	60, siltstone	5.43	12	[1]
LS	Ibid.	Babao section	37, siltstone	0.69	4	[1]

LS	Ibid.	Ibid.	34, siltstone	0.25	9	[1]
LS	Ibid.	Yujiabeigou section	13, mudstone and sandstone	10.3	27	[15]
LS	Xiaofengkou Fm.	Dafengkou section	49, mudstone	9.95	1	[7]
LS	Ibid.	Ibid.	44, siltstone and mudstone	8.65	13	[7]
LS	Ibid.	Ibid.	42, mudstone	9.95	7	[7]
LS	Ibid.	Ibid.	40, muddy siltstone	2.73	11	[7]
LS	Ibid.	Ibid.	37, silty mudstone	4.56	29	[7]
LS	Ibid.	Ibid.	35, mudstone	4.75	25	[7]
LS	Ibid.	Baojiagou section	33, sandstone	8.49	8	[7]
LS	Ibid.	Ibid.	32, silty mudstone	6.23	29	[7]
LS	Ibid.	Ibid.	30, mudstone and sandstone, with coal	5.92	12	[7]
LS	Ibid.	Ibid.	25, siltstone and mudstone	8.04	19	[7]
US	Yungaishan Fm.	Dafengkou section	88, siltstone and mudstone	9.02	12	[7]
US	Ibid.	Ibid.	81-82, sandstone, with siltstone	8.44	14	[7]
US	Ibid.	Ibid.	78, mudstone	1.17	15	[7]
US	Ibid.	Ibid.	76-77, mudstone, with coal	3.27	8	[7]
US	Ibid.	Ibid.	67, mudstone and siltstone	2.58	21	[7]
US	Ibid.	Pochi section	115, sandstone with siltstone	1	5	[7]
US	Ibid.	Ibid.	108, sandstone	2.98	4	[7]
US	Ibid.	Ibid.	107, sandy mudstone	6.37	6	[7]
US	Ibid.	Ibid.	103, siltstone	2.73	10	[7]
US	Ibid.	Dengcao	127, silty mudstone	4.36	4	[7]

		section				
US	Ibid.	Ibid.	126, mudstone	5.43	1	[7]
US	Ibid.	Ibid.	125, sandstone, with mudstone	5.85	2	[7]
US	Ibid.	Ibid.	124, dark gray mudstone	0.3	8	[7]
US	Upper Shihhotse Fm.	Babao section	71, dark gray siltstone	2.25	3	[1]
US	Ibid.	Ibid.	44, sandstone	38.87	5	[1]
US	Upper Shihhotse Fm.	Daoqing section	53, dark gray shale	3.0	10	[1]
US	Ibid.	Ibid.	50, black shale	1.0	3	[1]
US	Ibid.	Ibid.	34, dark gray shale	1.7	13	[1]
SJG	Sunjiagou Fm.	Wenquan section	91, mudstone	1.4	1	[16]
SJG	Ibid.	Ibid.	80, siltstone	1.2	1	[16]
SJG	Ibid.	Nantianmen coal mine	2, sandstone	13.3	7	[17]
SJG	Ibid.	Xigou-Zhangjiamen section	1, sandstone	15.3	3	[18]
SJG	Ibid.	Liulin-Wujiabu-Zhangjiayan section	8, sandstone	31.9	9	[18]
LJG	Liujiagou Fm.	Peijiashan section	19, sandstone and siltstone	28.5	1	[19]
LJG	Ibid.	Ibid.	18, sandstone and shale	10.7	6	[19]
LJG	Hongla Fm.	Yangshugou coal mine	4, conglomerate	20.8	11	[20]

HSG	Heshanggou Fm.	Hongyatoucun section	7, sandstone	2	6	[21]
Z&E	Ermaying Fm.	Qishuihe section	164, dark gray silty mudstone	7	4	[22]
Z&E	Ibid.	Ibid.	72, dark gray shale	8	8	[22]
Z&E	Ibid.	Laolaigou section	6, sandy mudstone and siltstone	1.6	20	[22]

* Based on the original descriptive literature. ** For the complete species list, please see Appendix 3. References: [1] Lin, 1990; [2] Chen, 2007; [3] He et al., 1990; [4] Pfefferkorn and Wang, 2007; [5] Zhou et al., 2017; [6] Wang et al., 2012; [7] Yang, 2006; [8] Niu, 1992; [9] Liu and Shen, 1978; [10] Sun et al., 1998; [11] Sun et al., 2012; [12] Lu, 1990; [13] He et al., 2015; [14] Chen, 2007; [15] Sun et al., 2016; [16] Wang, 1997; [17] Zhang et al., 1997; [18] Wang and Wang, 1986; [19] Wang and Wang, 1989; [20] Li et al., 2005; [21] Wang and Wang, 1990; [22] Huang and Zhou, 1980.

Table 2. Landscape-scale diversity of the eight intervals through the Permian to Middle Triassic of North China.

Interval	Patch code	Patch area*	Genus richness	Species richness	Representative sections**
TY interval	TY1	8.80	22	49	Dafengkou; Liangzhai
	TY2	8.75	44	98	Wuda; Hulstai; Fangtagou
	TY3	8.75	27	60	/
	TY4	2.69	23	52	Meiyaogou
	TY5	3.53	14	25	Weibei Coalfield
	TY6	7.01	33	68	/
	TY7	0.92	10	21	Babao
	Zibo	/	10	14	/
SX interval	SX1	8.01	83	271	Dafengkou; Shuoli
	SX2	4.45	68	211	Wuda; Hulstai; Shabatai; Heidaigou
	SX3	13.06	44	142	Qiaotou
	SX4	2.08	40	97	Daquan
	SX5	3.69	31	80	Weibei Coalfield
	SX6	6.64	30	71	Hesheng; Songshuzhen
	SX7	2.95	20	43	/
	Dongheishan	/	33	95	Dongheishan
LS interval	LS1	6.93	100	440	Dafengkou; Liuqiao
	LS2	12.55	74	218	Liulin-Wubu
	LS3	5.65	34	72	/
	LS4	10.52	34	60	/
	LS5	3.48	32	64	Weibei Coalfield
	LS6	4.06	28	55	Hulstai

	LS7	11.75	25	75	Yujiabeigou; Babao; Songshuzhen
	Dongheishan	/	22	40	/
US interval	US1	11.08	103	316	Dafengkou; Liuqiao
	US2	12.17	68	183	Liulin-Wubu
	US3	16.85	51	105	Dashankou
	US4	3.28	49	138	Babao; Daoqing
	US5	3.47	30	83	Weibei Coalfield
	US6	11.07	29	55	/
	US7	3.74	17	25	/
	US8	9.06	12	22	/
SJG interval	SJG1	4.51	21	34	/
	SJG2	3.38	35	50	Liulin-Wubu
	SJG3	2.26	11	15	Xigou-Zhangjiamen; Wenquan; Nantianmen
	SJG4	3.22	7	7	/
LJG interval	LJG1	5.52	15	23	Peijiashan
	LJG2	8.68	10	13	/
	LJG3	/	17	19	Yangshugou
HSG interval	HSG1	6.98	49	85	Hongyatou
	HSG2	3.86	15	23	Xigou
	HSG3	3.73	9	14	/
Z&E interval	Z&E1	7.85	40	64	Laolaigou
	Z&E2	6.35	17	23	Qishuihe
	Liaoning	/	37	58	/

* Unit: 10,000 km^2; ** For section location, see Fig. 4A-H and Appendix 4.

Table 3. Statistics of bed-scale and landscape-scale diversity of the eight intervals through the Permian to Middle Triassic of North China.

	Number of beds considered	Bed-scale species richness			Number of patches considered	Landscape-scale genus richness			Landscape-scale species richness		
		Range	Mean	Median		Range	Mean	Median	Range	Mean	Median
TY interval	13	2-40	9	5	8	10-44	23	23	14-98	48	51
SX interval	34	1-55	13	9	8	20-83	44	37	43-271	126	96
LS interval	19	1-29	12	9	8	22-100	44	33	40-440	128	68
US interval	18	1-21	8	7	8	12-103	45	40	22-316	116	94
SJG interval	5	1-9	4	3	4	7-35	19	16	7-50	27	25
LJG interval	3	1-11	6	6	3	10-17	14	15	13-23	18	19
HSG interval	1	6	6	6	3	9-49	24	15	14-85	41	23
Z&E interval	3	4-20	11	8	3	17-40	31	37	23-64	48	58

Table 4. Regional-scale diversity and heterogeneity index among sections of the eight intervals through the Permian to Middle Triassic of North China.

	Interval duration (million years)			Regional-scale diversity						Statistics of pairwise Heterogeneity Index between sections	
	Permian (Wang, 2010*)	Permian (Wu et al., 2021*)	Triassic	Genus richness	Species richness	Richness of foliage genera	Richness of foliage species	Percentage of non-foliage genera	Percentage of non-foliage species	Median ± SD**	Sections compared
TY interval	8	0.7	/	76	223	47	173	0.38	0.22	0.67 ± 0.18	8
SX interval	17	2.9	/	127	518	97	427	0.24	0.18	0.58 ± 0.18	16
LS interval	10	0.5	/	143	643	110	559	0.23	0.13	0.71 ± 0.15	9
US interval	10	14.1	/	152	597	121	530	0.20	0.11	0.74 ± 0.19	10
SJG interval	2	8	/	58	100	44	80	0.24	0.20	0.73 ± 0.33	4
LJG interval	/	/	2	32	52	25	43	0.22	0.17	0.75	2
HSG interval	/	/	3	52	96	39	76	0.25	0.21	1	2
Z&E interval	/	/	6	68	123	62	115	0.09	0.07	0.7	2

* Wang (2010) and Wu et al. (2021) presented different age determinations for the TY, SX, LS and US intervals, thus suggested different durations for these intervals. ** Standard deviation.

17

18 **Table 5.** Genus and species extinction, origination and turnover rates of the eight intervals through the

19 Permian to Middle Triassic of North China.

20

	Genus			Species		
	ER*	OR*	TR*	ER	OR	TR
TY/SX transition	0.28	0.57	0.63	0.48	0.77	0.81
SX/LS transition	0.33	0.41	0.54	0.51	0.60	0.72
LS/US transition	0.43	0.46	0.62	0.62	0.59	0.75
US/SJG transition	0.76	0.36	0.79	0.94	0.65	0.95
SJG/LJG transition	0.83	0.69	0.88	0.95	0.90	0.97
LJG/HSG transition	0.41	0.65	0.72	0.60	0.78	0.85
HSG/Z&E transition	0.54	0.63	0.74	0.81	0.85	0.91

21 * ER, extinction rates; OR, origination rates; TR, turnover rates.

22

Table 6. Surviving percentages in successive intervals of the genera and species that first occur in a given interval, through the Permian to Middle Triassic of North China.

	SX interval	LS interval	US interval	SJG interval	LJG interval	HSG interval	Z&E interval
TY interval	72/52*	67/45	57/30	29/5	11/2	12/2	14/4
SX interval		67/49	51/32	20/4	9/1	11/2	13/2
LS interval			57/38	21/5	8/1	11/1	15/2
US interval				24/6	9/1	11/2	15/3
SJG interval					17/5	22/5	29/7
LJG interval						59/4	53/19
HSG interval							48/19

* Surviving percentage of genera/species.

Table 7. The values of three attributes of networks for patch-plant data matrices of the eight intervals through the Permian to Middle Triassic of North China.

	Average Degree	Graph Density	Modularity
TY interval	2.222	0.028	0.283
SX interval	2.575	0.019	0.248
LS interval	2.278	0.015	0.29
US interval	2.22	0.014	0.295
SJG interval	1.224	0.021	0.471
LJG interval	1.2	0.035	0.426
HSG interval	1.314	0.026	0.311
Z&E interval	1.288	0.018	0.403

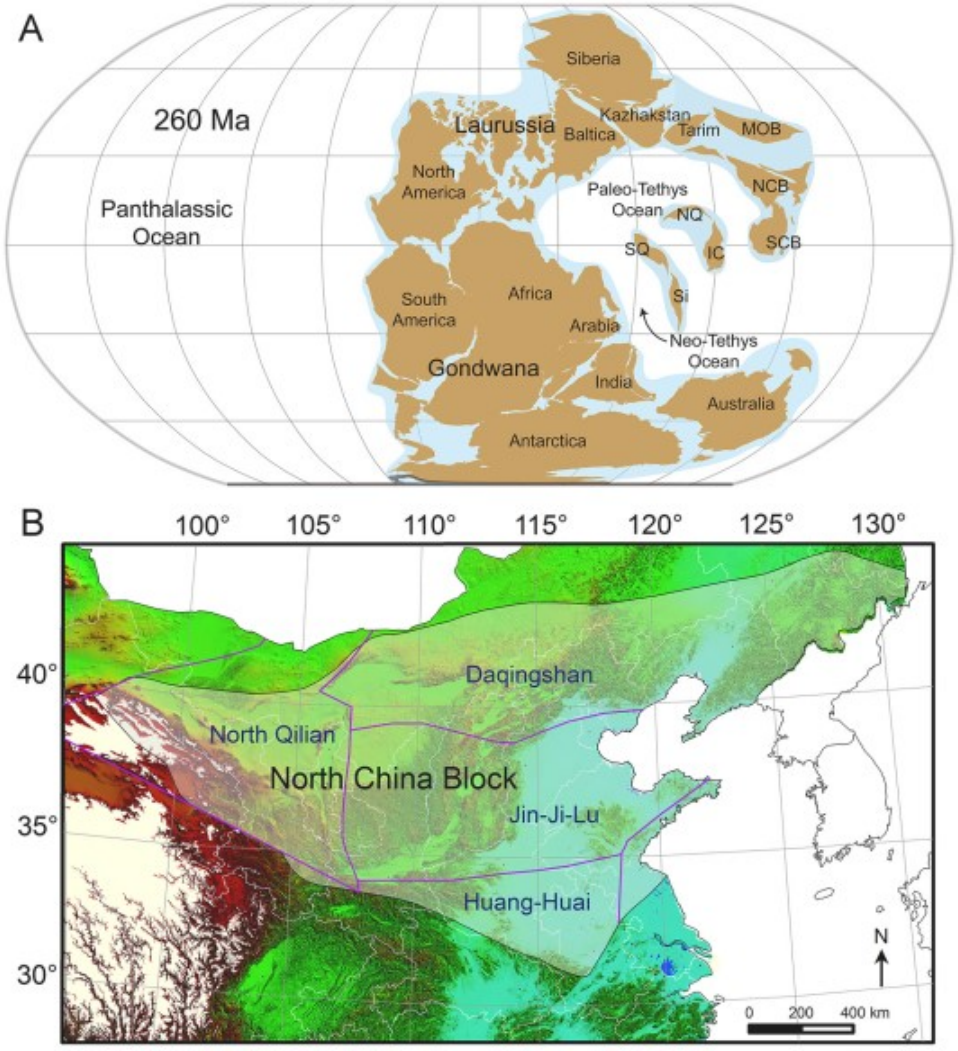
A
260 Ma
Panthalassic Ocean
Siberia
Laurussia
Kazhakstan
Baltica
Tarim
MOB
North America
Paleo-Tethys Ocean
NCB
NQ
SQ
IC
SCB
Si
South America
Africa
Arabia
Neo-Tethys Ocean
Gondwana
India
Australia
Antarctica
B
100°
105°
110°
115°
120°
125°
130°
40°
35°
30°
Daqingshan
North Qilian
North China Block
Jin-Ji-Lu
Huang-Huai
N
0
200
400 km

<table>
<tr><th colspan="2">Wang (2010)</th><th>Wu et al. (2021)</th><th colspan="6">this paper</th></tr>
<tr><th colspan="3"></th><th>Jin-Ji-Lu</th><th>Huang-Huai</th><th colspan="2">North Qilian</th><th colspan="2">Daqingshan</th></tr>
<tr><td rowspan="3">Triassic</td><td>Anisian</td><td>Anisian</td><td>Zhifang Fm. / Ermaying Fm.</td><td>Ermaying Fm.</td><td colspan="2">Dingjiayao Fm.</td><td rowspan="2">Xidagou Group</td><td rowspan="2">Tanzhesi Fm.</td><td>Linjia Fm.</td></tr>
<tr><td>Olenekian</td><td>Olenekian</td><td>Heshanggou Fm.</td><td>Heshanggou Fm.</td><td colspan="2" rowspan="2">Lower Xidagou Group</td><td rowspan="2">Hongla Fm.</td></tr>
<tr><td>Induan</td><td>Induan</td><td>Liujiagou Fm.</td><td>Liujiagou Fm.</td></tr>
<tr><td rowspan="8">Permian</td><td>Changhsingian</td><td>Wuchiapingian to Changhsingian</td><td>Sunjiagou Fm.</td><td>Sanfengshan Fm.</td><td colspan="2"></td><td colspan="2">Dabeisi Fm.</td><td>Hamashan Fm.</td></tr>
<tr><td rowspan="3">Capitanian to Wuchiapingian</td><td>Kungurian</td><td rowspan="3">Upper Shihhotse Fm.</td><td rowspan="3">Yungaishan Fm.</td><td rowspan="2">Daquan Fm.</td><td rowspan="2">Sunan Fm.</td><td rowspan="2">Shuangquan Fm.</td><td rowspan="4">Shihhotse Fm.</td></tr>
<tr><td>Artinskian</td></tr>
<tr><td>Sakmarian</td><td>Hongquan Fm.</td><td>Yaogou Fm.</td><td>Hongmiaoling Fm.</td></tr>
<tr><td>Roadian to Wordian</td><td rowspan="3">Asselian</td><td>Lower Shihhotse Fm.</td><td>Xiaofengkou Fm.</td><td>Upper Shandan Group</td><td>Dahuanggou Fm.</td><td>Lower Shihhotse Fm.</td></tr>
<tr><td>Artinskian to Kungurian</td><td>Shanxi Fm.</td><td>Shenhou Fm.</td><td>Lower Shandan Group</td><td>Tongwei Fm.</td><td>Shanxi Fm.</td><td>Shanxi Fm.</td></tr>
<tr><td>Asselian to Sakmarian</td><td>Taiyuan Fm. (middle-upper)</td><td>Zhutun Fm.</td><td></td><td>Taiyuan Fm. (middle-upper)</td><td>Taiyuan Fm. (middle-upper)</td><td>Taiyuan Fm. (middle-upper)</td></tr>
</table>

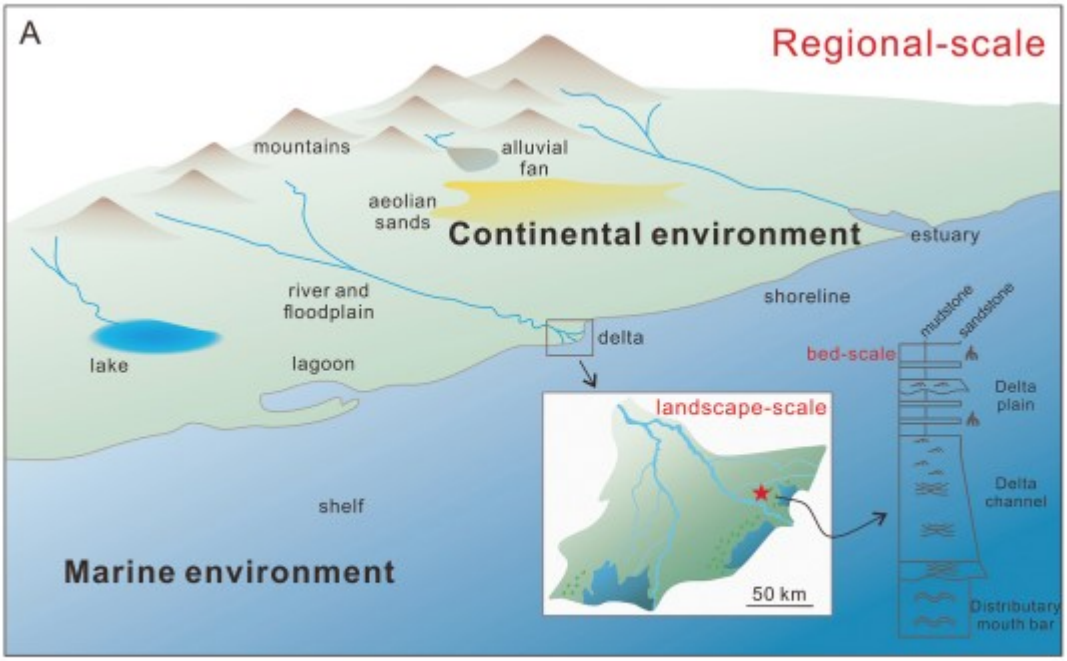
A
Regional-scale
mountains
alluvial fan
aeolian sands
Continental environment
estuary
river and floodplain
shoreline
lake
lagoon
delta
bed-scale
mudstone
sandstone
Delta plain
landscape-scale
Delta channel
shelf
Marine environment
50 km
Distributary mouth bar

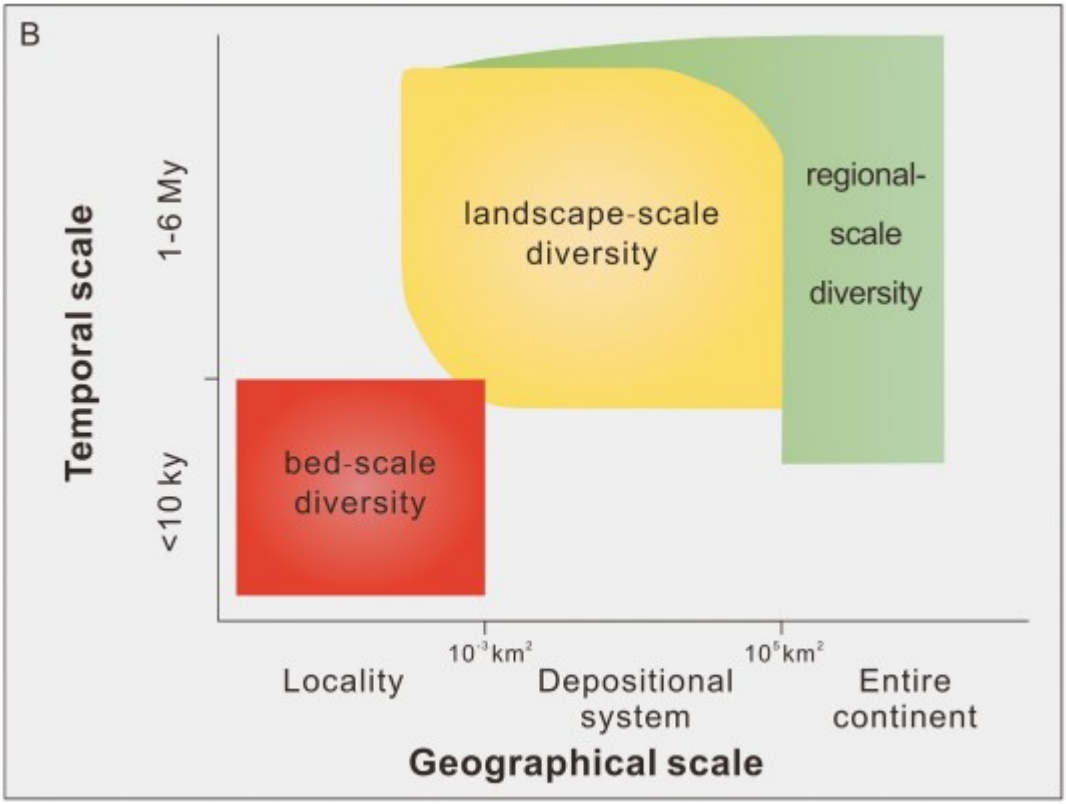
B
Temporal scale
1-6 My
<10 ky
landscape-scale diversity
regional-scale diversity
bed-scale diversity
10^{-3} km^2
10^{5} km^2
Locality
Depositional system
Entire continent
Geographical scale

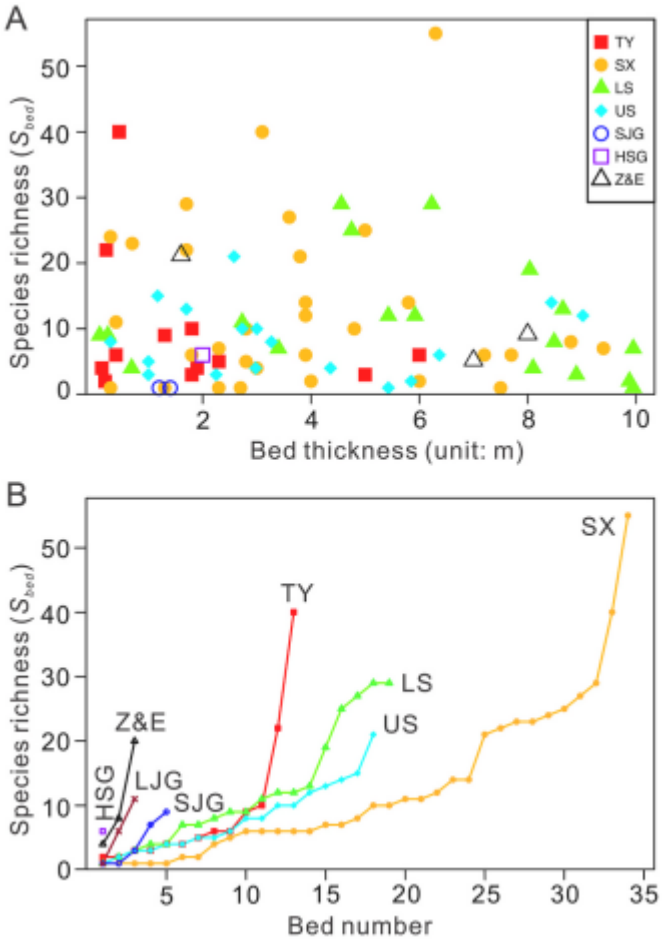
A
Species richness (S_{bed})
Bed thickness (unit: m)
TY
SX
LS
US
SJG
HSG
Z&E
B
Species richness (S_{bed})
Bed number
SX
TY
LS
US
Z&E
LJG
SJG
HSG

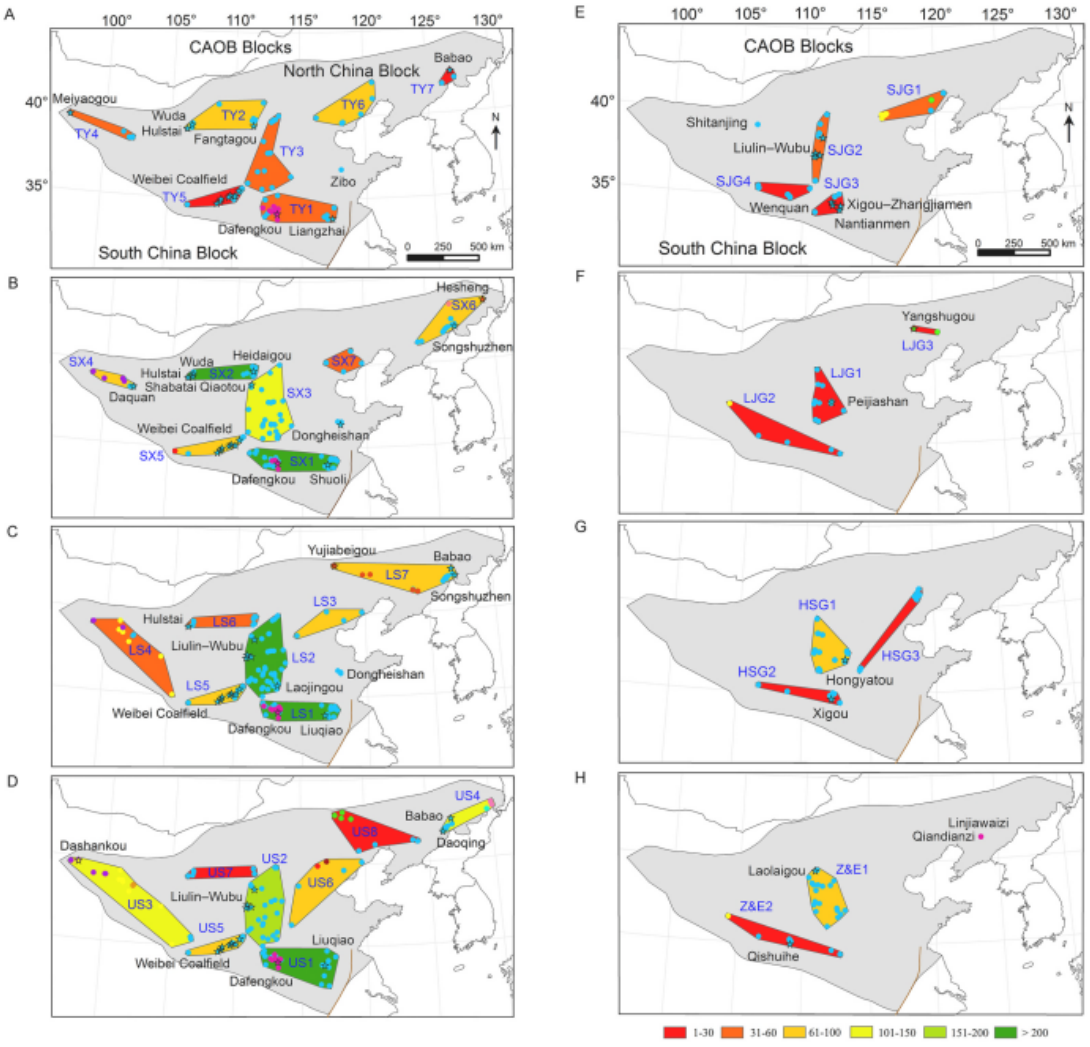
A
CAOB Blocks
North China Block
South China Block
Babao
TY7
TY6
Meiyaogou
Wuda
Hulstai
TY4
TY2
Fangtagou
TY3
Weibei Coalfield
TY5
Zibo
TY1
Dafengkou
Liangzhai
100°
105°
110°
115°
120°
125°
130°
40°
35°
N
0 250 500 km
B
Hesheng
SX6
Songshuzhen
SX4
Wuda
Heidaigou
SX7
Hulstai
SX2
Shabatai Qiaotou
Daquan
SX3
Weibei Coalfield
Dongheishan
SX5
SX1
Dafengkou
Shuoli
C
Yujiabeigou
Babao
LS7
Songshuzhen
LS3
Hulstai
LS6
LS4
Liulin–Wubu
LS2
Dongheishan
LS5
Laojingou
Weibei Coalfield
LS1
Dafengkou
Liuqiao
D
US4
Babao
US8
Daoqing
Dashankou
US2
US7
US6
US3
Liulin–Wubu
US5
Liuqiao
Weibei Coalfield
US1
Dafengkou
E
CAOB Blocks
South China Block
SJG1
Shitanjing
Liulin–Wubu
SJG2
SJG4
SJG3
Wenquan
Xigou–Zhangjiamen
Nantianmen
F
Yangshugou
LJG3
LJG1
LJG2
Peijiashan
G
HSG1
HSG3
HSG2
Hongyatou
Xigou
H
Linjiawaizi
Qiandianzi
Laolaigou
Z&E1
Z&E2
Qishuihe
1-30
31-60
61-100
101-150
151-200
> 200

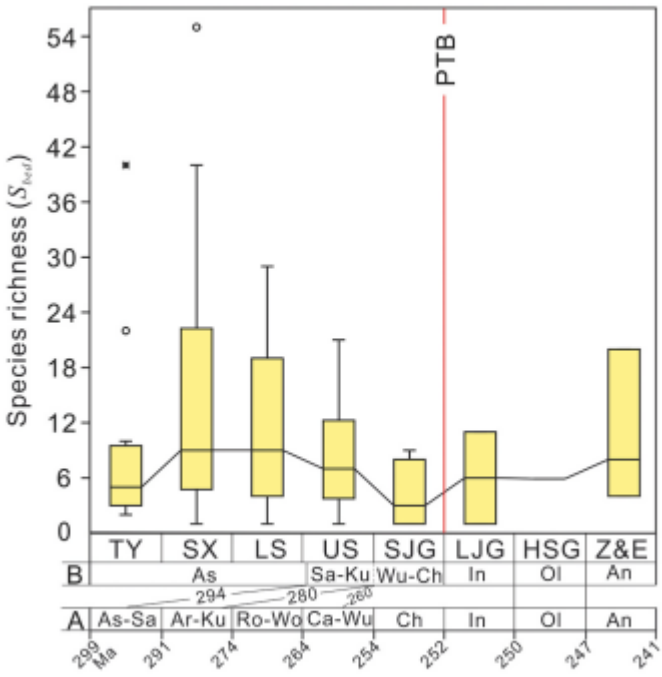
Species richness (S_{bul})
54
48
42
36
30
24
18
12
6
0
PTB
TY
SX
LS
US
SJG
LJG
HSG
Z&E
B
As
Sa-Ku
Wu-Ch
In
Ol
An
294
280
260
A
As-Sa
Ar-Ku
Ro-Wo
Ca-Wu
Ch
In
Ol
An
299
Ma
291
274
264
254
252
250
247
241

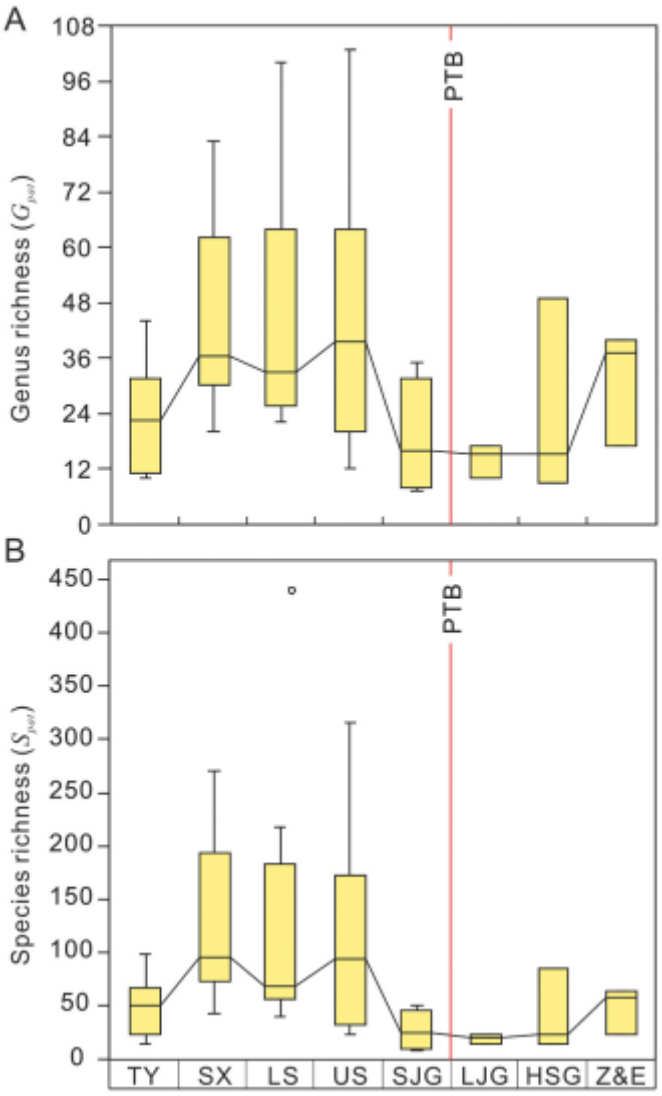
A
Genus richness (G_{pwt})
108
96
84
72
60
48
36
24
12
0
PTB
B
Species richness (S_{pwt})
450
400
350
300
250
200
150
100
50
0
PTB
TY
SX
LS
US
SJG
LJG
HSG
Z&E

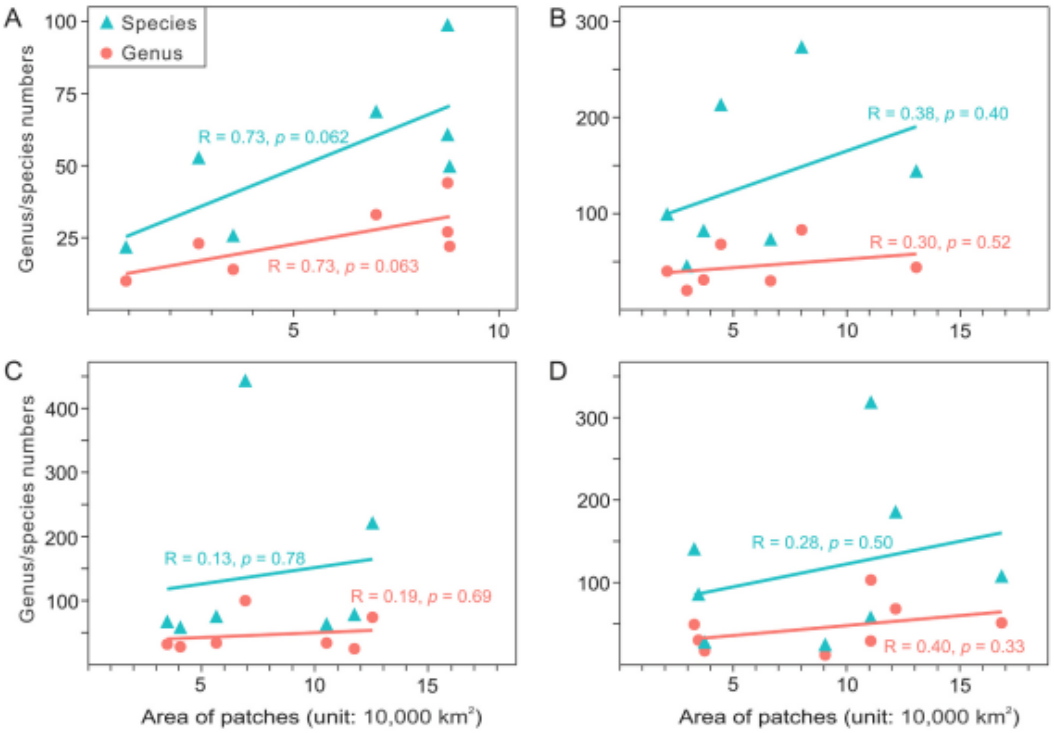
A
Species
Genus
Genus/species numbers
R = 0.73, p = 0.062
R = 0.73, p = 0.063
B
R = 0.38, p = 0.40
R = 0.30, p = 0.52
C
Genus/species numbers
R = 0.13, p = 0.78
R = 0.19, p = 0.69
Area of patches (unit: 10,000 km²)
D
R = 0.28, p = 0.50
R = 0.40, p = 0.33
Area of patches (unit: 10,000 km²)

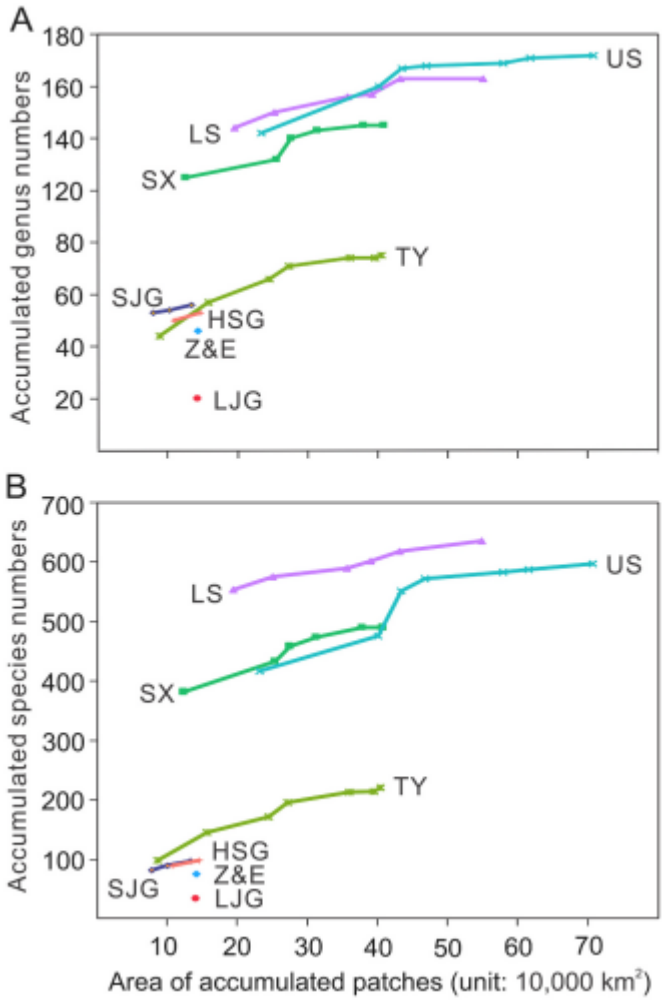
A
Accumulated genus numbers
180
160
140
120
80
60
40
20
US
LS
SX
TY
SJG
HSG
Z&E
LJG
B
Accumulated species numbers
700
600
500
400
300
200
100
LS
US
SX
TY
HSG
Z&E
SJG
LJG
10
20
30
40
50
60
70
Area of accumulated patches (unit: 10,000 km²)

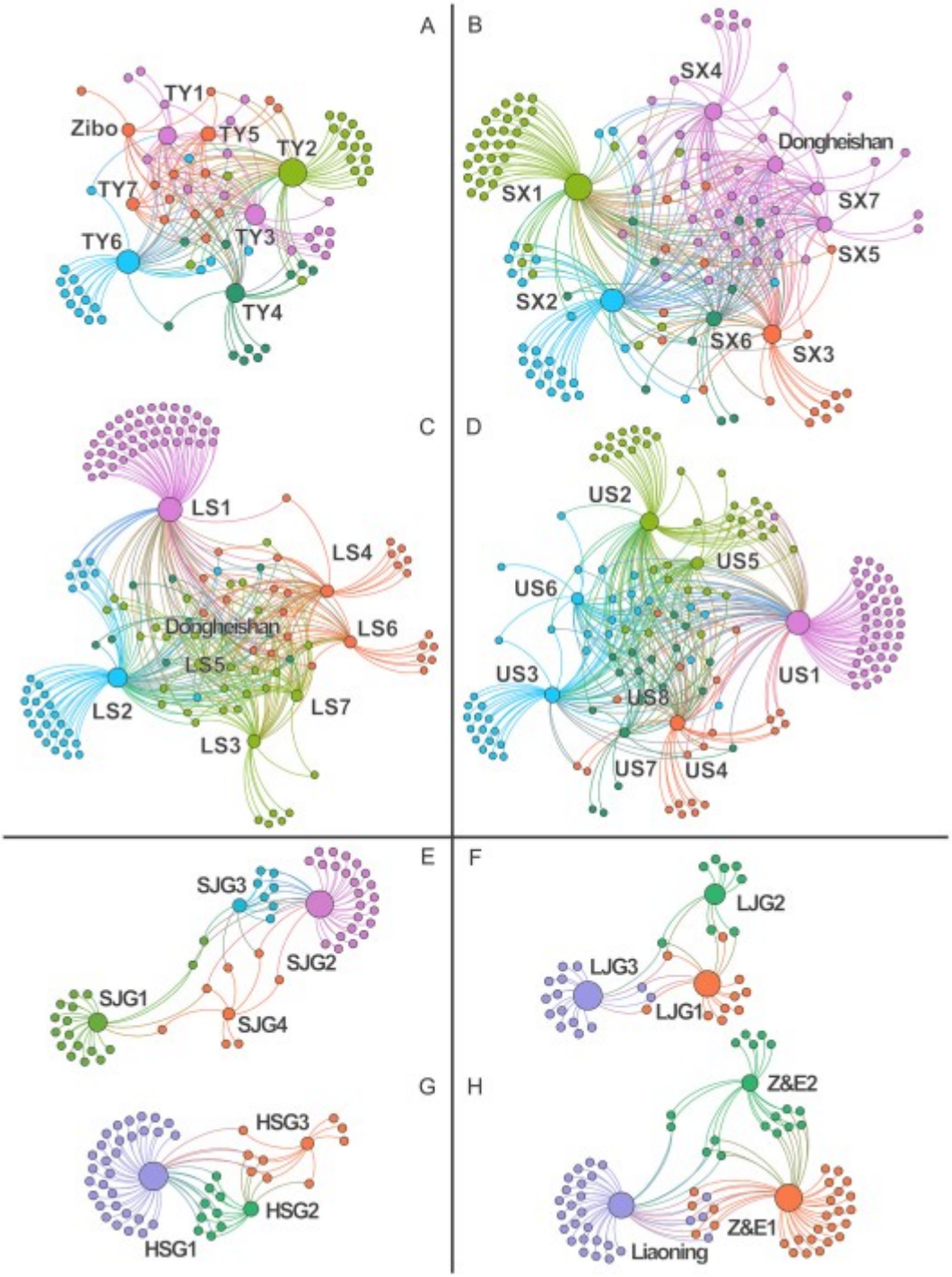
A
Zibo
TY1
TY5
TY2
TY7
TY3
TY6
TY4
B
SX4
Dongheishan
SX1
SX7
SX5
SX2
SX6
SX3
C
LS1
LS4
Dongheishan
LS6
LS5
LS2
LS7
LS3
D
US2
US5
US6
US1
US3
US8
US7
US4
E
SJG3
SJG2
SJG1
SJG4
F
LJG2
LJG3
LJG1
G
HSG3
HSG2
HSG1
H
Z&E2
Z&E1
Liaoning

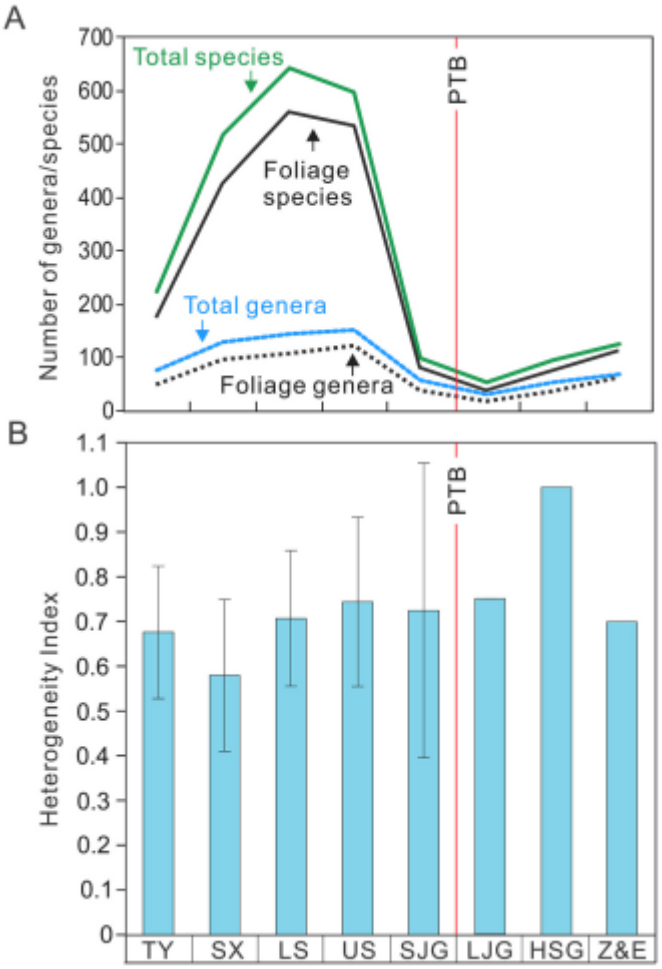
A
Number of genera/species
700
600
500
400
300
200
100
0
Total species
Foliage species
Total genera
Foliage genera
PTB
B
Heterogeneity Index
1.1
1.0
0.9
0.8
0.7
0.6
0.5
0.4
0.3
0.2
0.1
0
PTB
TY
SX
LS
US
SJG
LJG
HSG
Z&E

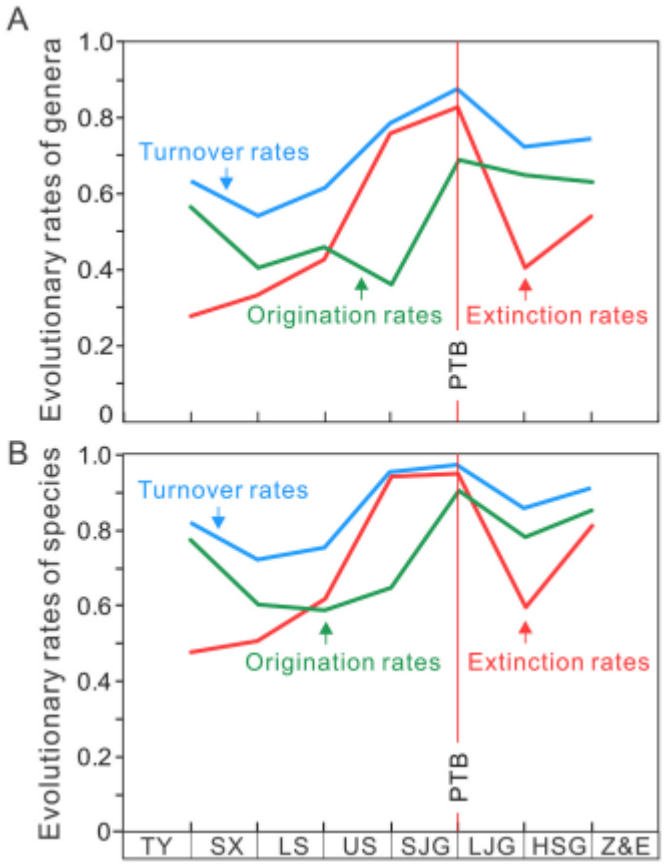
A
Evolutionary rates of genera
1.0
0.8
0.6
0.4
0.2
0
Turnover rates
Origination rates
Extinction rates
PTB
B
Evolutionary rates of species
1.0
0.8
0.6
0.4
0.2
0
Turnover rates
Origination rates
Extinction rates
PTB
TY
SX
LS
US
SJG
LJG
HSG
Z&E

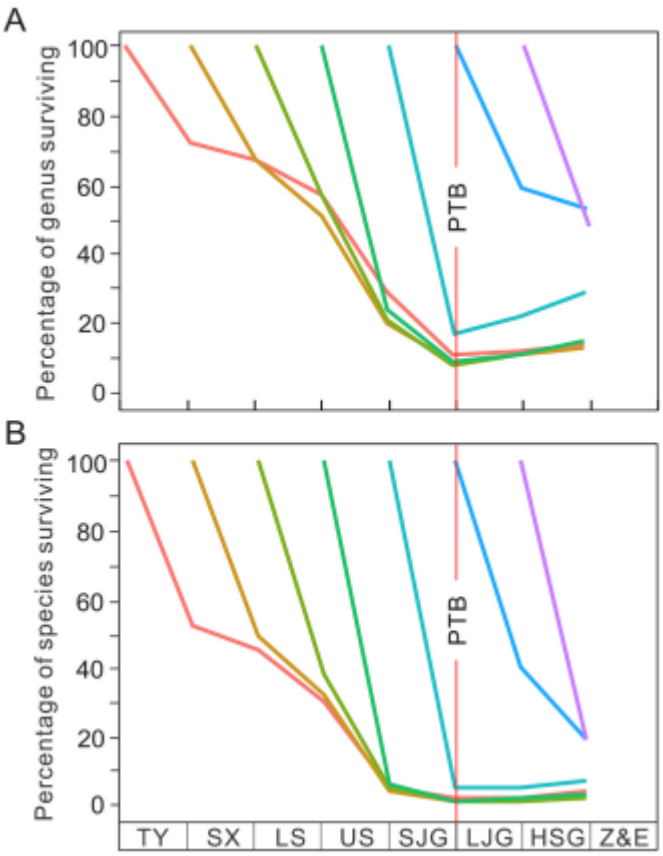
A
Percentage of genus surviving
100
80
60
40
20
0
PTB
B
Percentage of species surviving
100
80
60
40
20
0
PTB
TY
SX
LS
US
SJG
LJG
HSG
Z&E

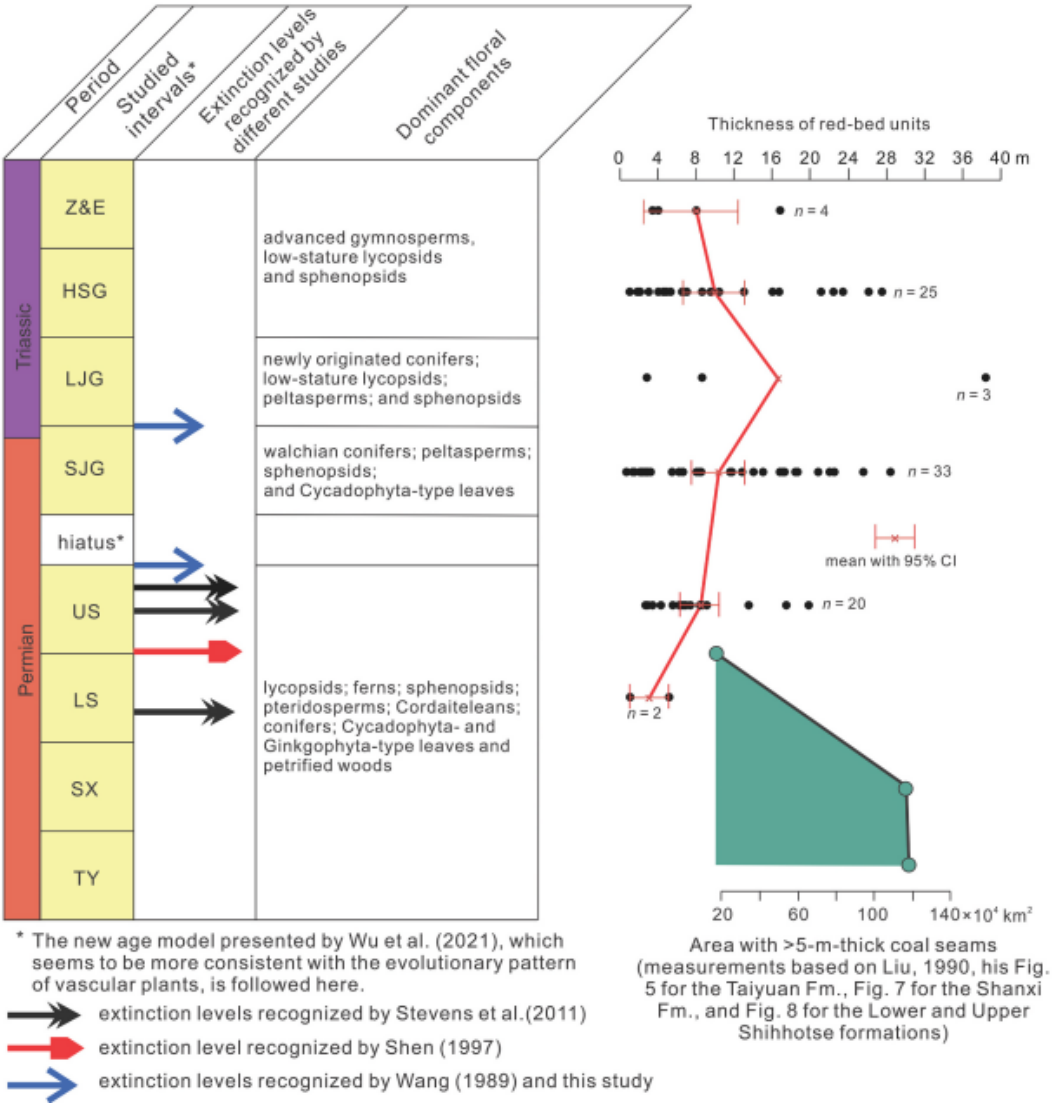
Period
Studied intervals*
Extinction levels recognized by different studies
Dominant floral components
Triassic
Permian
Z&E
HSG
LJG
SJG
hiatus*
US
LS
SX
TY
advanced gymnosperms, low-stature lycopsids and sphenopsids
newly originated conifers; low-stature lycopsids; peltasperms; and sphenopsids
walchian conifers; peltasperms; sphenopsids; and Cycadophyta-type leaves
lycopsids; ferns; sphenopsids; pteridosperms; Cordaiteleans; conifers; Cycadophyta- and Ginkgophyta-type leaves and petrified woods
Thickness of red-bed units
0 4 8 12 16 20 24 28 32 36 40 m
n = 4
n = 25
n = 3
n = 33
mean with 95% CI
n = 20
n = 2
20 60 100 140×10⁴ km²
* The new age model presented by Wu et al. (2021), which seems to be more consistent with the evolutionary pattern of vascular plants, is followed here.
extinction levels recognized by Stevens et al.(2011)
extinction level recognized by Shen (1997)
extinction levels recognized by Wang (1989) and this study
Area with >5-m-thick coal seams (measurements based on Liu, 1990, his Fig. 5 for the Taiyuan Fm., Fig. 7 for the Shanxi Fm., and Fig. 8 for the Lower and Upper Shihhotse formations)